GEAP-4360
AEC RESEARCH AND
DEVELOPMENT REPORT
SEPTEMBER 16, 1963

ACCENT ON VALUE

MASTER

FUEL FAILURE EXAMINATIONS AND ANALYSES IN THE HIGH POWER DENSITY PROGRAM

Facsimile Price $ 3.60
Microfilm Price $ 3.05

Available from the
Office of Technical Services
Department of Commerce
Washington 25, D. C.

By
W.H. ARLT
S.R. VANDENBERG

U.S. ATOMIC ENERGY COMMISSION
CONTRACT AT(04-3)-361

VALLECITOS ATOMIC LABORATORY
GENERAL ELECTRIC
ATOMIC POWER EQUIPMENT DEPARTMENT
SAN JOSE, CALIFORNIA

GEAP-4360
Informal AEC Research
and Development Report
September 1963

FUEL FAILURE EXAMINATIONS AND ANALYSES IN THE HIGH POWER DENSITY PROGRAM

by

W. H. Arlt

S. R. Vandenberg

Prepared For

U. S. Atomic Energy Commission

Contract AT(04-3)-361

Printed in U.S.A. ~~Price $2.00~~. Available from the Office of Technical Services, Department of Commerce, Washington 25, D. C.

ATOMIC POWER EQUIPMENT DEPARTMENT

GENERAL ELECTRIC

SAN JOSE, CALIFORNIA

1401-TIO-2

LEGAL NOTICE

This report was prepared as an account of Government sponsored work. Neither the United States, nor the Commission, nor any person acting on behalf of the Commission:

A. Makes any warranty or representation, expressed or implied, with respect to the accuracy, completeness, or usefulness of the information contained in this report, or that the use of any information, apparatus, method, or process disclosed in this report may not infringe privately owned rights; or

B. Assumes any liabilities with respect to the use of, or for damages resulting from the use of any information, apparatus, method, or process disclosed in this report.

As used in the above, "person acting on behalf of the Commission" includes any employee or contractor of the Commission, or employee of such contractor, to the extent that such employee or contractor of the Commission, or employee of such contractor prepares, disseminates, or provides access to, any information pursuant to his employment or contract with the Commission, or his employment with such contractor.

TABLE OF CONTENTS

LIST OF ILLUSTRATIONS

LIST OF ILLUSTRATIONS (Continued)

LIST OF TABLES

1.0 INTRODUCTION

The High Power Density Development Project includes a comprehensive fuel development program aimed primarily at developing and demonstrating the performance of a nuclear reactor core having a high power density, long fuel life, and low fuel fabrication cost. As part of the program, Type 304 stainless steel clad UO_2 fuel rods are being irradiated in the Vallecitos Boiling Water Reactor. The fuel development portions of the High Power Density Program are reported here and are designated as Tasks 1A and 1B.

The objective of the Task 1A program is to evaluate the feasibility and study the performance of a partial reactor core (24 assemblies) operating in the VBWR at high power density conditions utilizing fuel manufactured by current fabricating processes. The fuel for Task 1A irradiation was designed for operation in the VBWR at 90 Kw/l average power density, 425,000 Btu/hr-ft^2 peak surface heat flux, and 10,000 MWD/T average burnup. Irradiation of Task 1A fuel started in October, 1960.

The objective of Task 1B is to investigate fabrication processes which offer potentially lower fabrication costs than current processes, and to subsequently fabricate fuel by these processes for operational testing in the VBWR. Twelve fuel assemblies have been fabricated to date for operation in the VBWR at 80 Kw/l average power density, 480,000 Btu/hr-ft^2 peak heat flux and 10,000 MWD/T average exposure. Irradiation of Task 1B fuel started in April, 1961.

In addition to the objectives stated above, Tasks 1A and 1B include investigation of the feasibility of thinning the wall of stainless steel cladding as a means of improving the neutron economy and fuel cycle costs of stainless steel clad fuel. Thus, a portion of the program has included the testing of fuel clad designs which represent a departure from the conventional "free-standing"* stainless steel clad design to date in operating power reactors.

During the months of April, July, August and September, 1962, service failures in eight Task 1A type fuel rods occurred during operation. In September, 1962, the VBWR was shut down for an extended period until January, 1963. Subsequent fuel rod service failures occurred during the months of February, March, April, May and June in assemblies from both Task 1A and 1B. In June, 1963, there were nine Task 1A fuel assemblies and four Task 1B assemblies operating in the VBWR, all other assemblies were either confirmed or suspected of having failed fuel rods.

The purpose of this progress report is to describe the post-irradiation examinations performed through June, 1963, on the fuel failures. In addition, the report presents a preliminary analysis of fuel design and operational data permitting tentative conclusions regarding possible mechanisms of Type 304 stainless steel fuel failure.

---

* "Free-standing" refers to a clad tube thick enough to withstand coolant pressure without collapsing against the UO_2.

2.0 SUMMARY

The High Power Density Project includes a comprehensive fuel development program which has the objective of developing and demonstrating the performance of a nuclear reactor core having a high power density, long fuel life, and low fabrication cost. The fuel program is made up of two principal tasks. Task 1A consists of irradiation tests in the VBWR of Type 304 stainless steel clad, UO_2 pellet type fuel rods fabricated by current commercial processes. Task 1B consists of the investigation of lower cost fabrication processes and the irradiation testing of fuel elements fabricated by these processes. Both tasks include the investigation of the feasibility of use of thin-wall stainless steel cladding as a means of improving the neutron economy and fuel cycle costs of stainless steel clad fuel.

The design variables for the Task 1A fuel rods include clad wall thickness, pellet-to-clad gap, and clad cold work. The Task 1B fuel rods, which include variations in clad wall thickness, clad cold work, and UO_2 density, are fabricated by the pellet process and by powder compaction processes such as hot swaging, cold swaging, vibrational compaction, and tandem rolling.

Irradiation of the Task 1A fuel assemblies in the VBWR was initiated in September, 1960. Subsequently, Task 1B fuel assemblies were inserted in the VBWR as various fabrication processes and design concepts were investigated. All assemblies operated satisfactorily until April, 1962, when a fuel cladding failure was experienced in Assembly HPD 2D of the Task 1A fuel assemblies. Subsequently, additional failures have occurred in fuel rods in both Task 1A and 1B. At the present time 13 assemblies are operational with all other assemblies classified as containing one or more failed rods. Of the rods remaining under irradiation, the average burnup in the leading rod currently is approximately 9,500 MWD/T. As of this date, cladding failures have occurred in twenty-two rods of approximately 700 fuel rods which have been irradiated. Twenty of the failures occurred in cold worked tubing and two in tubing procured commercially as annealed materials.

Visual and detailed examination of failed rods indicates the following:

1. The cladding failures are cracks which vary in size from small, barely visible hairline cracks to large cracks in which the UO_2 is exposed to the reactor coolant.

2. In all cases but two, the cracks are longitudinal to the axis of the fuel rod. One annealed rod in assembly HPD 4E and one in assembly HPD 6S exhibited both circumferential and longitudinal cracks.

3. Metallographic examinations indicate that the cracks are intergranular and start at the outside surface. There is evidence of intergranular corrosion, strongly accelerated by stress. Optical microscopy does not reveal any evidence of sensitization in the grain boundaries.

4. In all cases, the failures occurred in the high heat flux region of the fuel rods.

The mode of failure, intergranular cracking of nonsensitized Type 304 stainless steel in a high purity water environment, has not been reported to have occurred previously in an ex-reactor application. However, in addition to the VBWR experience, similar type failures of highly stressed Type 304 stainless steel have been reported to have occurred in a pressurized water reactor environment.

Evaluation of the failures conducted thus far indicates the operating stress level in the clad is a significant factor in causing the cracking. However, the relative contributions of other potential effects such as time at temperature in the coolant environment, effects of irradiation, and effects of fuel rod power cycling have not yet been determined.

At the present time, it appears the maximum lifetime of stainless steel clad fuel in water reactor applications can be attained by operating with as low a clad stress level as possible. Intergranular stress-influenced corrosion cracking of Type 304 stainless steel cladding occurs in fuel assemblies with increasing exposure to HPD test conditions in the following order:

Pellet Fuel

1. Swaged pellet fuel, starting with cold worked or annealed tubing, 8-12 mils thick. Failure range: approx. 4000-5500 MWD/T average, experienced by the "D" assemblies and assemblies 3S and 6S.

2. Swaged pellet fuel, starting with cold worked tubing, 14 mils thick. Failure range: approx. 5000-8000 MWD/T average, experienced by the "G" assemblies.

3. Standard pellet fuel, starting with cold worked tubings 14 mils thick. Failure range: approx. 6000-8500 MWD/T average, experienced by the "E" group and assembly 2F.

4. Standard pellet fuel, starting with annealed cladding, 14 mils thick. Failure: approx. 8400 MWD/T average (as of June 30 1963), experienced by assembly 4E.

5. Standard pellet fuel, starting with cold worked or annealed cladding, 17-20 mils thick, has experienced no failures (as of June 30, 1963). Exposure ranges known 4700 to 6700 MWD/T average.

Powder Fuel

1. Cold swaged powder fuel with cold worked cladding, 10-16 mils thick, and density of 90-94 percent. Failure range: approx. 3800-4500 MWD/T average, experienced by assemblies 2S and 7S.

2. Hot swaged, tandem-rolled, and vibratory compacted fuel rods, 12-16 mils thick, have experienced no failures (as of June 30, 1963). Exposure ranges from 3800 to 4500 MWD/T average.

3.0 DISCUSSION

The current status of evaluation of the mechanism of clad failures does not provide a full understanding of the contributing factors and their relative magnitudes of contribution. The intergranular cracking of the Type 304 stainless steel cladding appears to be caused by preferential corrosion of the grain boundaries and appears to be strongly sensitive to the operating stress level of the cladding. The effects of other potentially contributing factors such as time-at-temperature in a reactor water environment, radiation effects, metallurgical structure, and fuel rod power cycling are not known at this time.

Intergranular cracking of stabilized austenitic stainless steels has been reported by Wanklyn and Jones[1] and Snowden[2] to have occurred in caustic solutions such as NaOH and KoH. However, the intergranular cracking of nonsensitized Type 304 stainless steel in relatively high purity water is known to have occurred only in a reactor environment. In addition to the VBWR experience, intergranular cracking of highly stressed, nonsensitized Type 304 stainless steel is reported to have occurred in a pressurized water reactor environment.[3] High stress level appears to be a common factor in the cracking of stainless steel in both PWR and BWR environments.

Continued investigation of the performance of stainless steel cladding is necessary to determine the cause or causes of failure. It is expected the performance of other stainless steel clad fuel rods in the VBWR[4][5] will provide useful additional data.

Investigation of the potential contributing factors has revealed the following:

1. Indications of Preferential Corrosion Attack

   The observation that failures have occurred in the grain boundaries and to a slight degree along slip planes and twin boundaries of the stainless steel microstructure suggests that corrosion attack is taking place. This is coupled with the evidence that no signs of deformation by yielding are present. Studies are in progress examining the clad structure using the techniques of electron microscopy. Dislocation concentrations and intergranular constituents, not detectable by the optical microscope, will be sought. Also it is intended to establish whether a corrosion product exists in the cracks and, if present, to identify it.

2. Effect of Clad Stresses

   All but two failures have occurred longitudinally, normal to the highest theoretical stress (hoop stress). Tensile stresses on the outer fibers of the clad during operation in the reactor are composed of the additive stresses resulting from internal fission gas pressure, from interference between the clad and pellet upon heating to operating temperature, from thermal stresses resulting from the temperature drop across the clad, and from the residual stresses present in the tubing as received from the tubing supplier. Recent investigations made by Lees,[18, 31] indicate residual stresses present in commercially annealed and

cold worked 304 stainless steel can be as high as 20,000 psi and 40,000 psi, respectively. In the commercially annealed material, residual tensile stress in the outer fibers of the clad measured between 10,000 psi and 20,000 psi. For cold worked tubing, residual tensile stresses of between 30,000 and 40,000 psi were measured in the outer fibers. A certain level of tensile stress will always be present at operating temperature in fuel cladding when commercially available material is used, unless the material is given a dead anneal heat treatment prior to irradiation. Additional localized tensile stresses can be imposed by elastic deformation of the clad by the external coolant pressure due to clad tube ovality. However, failure cannot be attributed to stress alone because of the intergranular nature of the cracks and absence of evidence of plastic deformation and transgranular cracking if stresses had been high enough to cause a typical mechanical failure. The evidence of appreciable ductility in the tensile and burst tests of material from assembly 1G supports this view.

The initial, as-fabricated pellet-to-clad gap is an important factor in establishing the degree of UO_2-clad interference and resultant clad stress that will occur when the fuel rod is brought to operating temperature. Assuming the t/D is a measure of clad stress for a particular UO_2-clad cold gap, a proposed family of curves is shown in Figure 50 in which lifetime-to-failure is plotted against t/D for various initial gap conditions. There are several points with which to plot the curves for the zero or very small gap fuel rods. These are the rods in which UO_2-clad interference stresses are large in magnitude. Inasmuch as the number of datum points for the five mil gap, essentially zero interference stress, rods does not permit plotting of curves, they are assumed at this time to be parallel to the small gap curves. Additional points are shown for fuel rod types which have had no failures. Until more datum points are obtained, the curves in Figure 50 must be considered preliminary in nature. At this point, they tend to confirm that the time-to-failure is a function of clad stress level and that the direction for longer fuel life is to reduce the clad operating stresses.

3. Effects of Radiation

The exposure of the cladding to fast neutron flux may be a contributing factor in causing clad failure. However, the high strength and retention of appreciable ductility in the uncracked material of the 1G assembly indicates the direct effect of irradiation is probably a contributing but not a primary factor.

4. Effects of Time in High Temperature Water Environment

It appears that the chemical environment, peculiar to the reactor coolant and the effects of irradiation, is a significant factor in initiating and propagating corrosion attack. The intergranular nature of the clad cracks indicates preferential corrosion attack with the presence of high stresses being a necessary or accelerating effect. A tentative correlation is proposed as shown in Figure 50 combining the effects of stress, corrosion and time. The variables in Figure 50 represent:

a. Thickness-to-diameter ratio (t/D)

This parameter is a rough measure of the clad stress level at operating conditions. t/D is also fairly representative of the thickness of clad material present to resist a "corrosive" media. It is from these considerations that time-to-failure might be correlated with t/D.

b. Time-at-Temperature (Hours Critical)

For the VBWR the number of hours the fuel is recorded to have been critical is a very close measure of time at temperature. This also is representative of the actual time subjected to the effects of neutron flux and coolant environment. The time the cladding endures peak stresses (or stresses within 10 percent of maximum) may be as low as 10 percent of the time critical. The correlation drawn applies to the HPD fuel exposed in the VBWR. It is not implied that it should apply to fuel in other reactors with different design conditions.

A recent survey indicates the irradiation tests conducted in the VBWR comprise the most extensive irradiation testing experience of Type 304 stainless steel clad, UO_2 fuel rods under actual water reactor temperature and pressure conditions.[3] A very significant result thus far of the VBWR fuel tests is the indication of the susceptibility of austenitic stainless steel clad to failure by intergranular cracking.

At the present time, clad performance evaluation indicates the maximum lifetime of stainless steel clad fuel in water reactor applications can be attained by operating with as low a clad stress level as possible. This implies longer fuel life can be attained with free-standing stainless steel clad fuel than with thin-walled clad fuel.

Preliminary results of current investigations conducted as a part of the superheat project indicate improvements in the performance of austenitic stainless steel cladding can be made by changes in impurity levels and by the use of higher nickel alloys such as Incoloy. On the basis of favorable performance results in irradiation tests under superheated steam conditions,[7] the irradiation testing of an Incoloy clad fuel assembly in the VBWR was initiated recently.[8]

The neutron economy of Incoloy is only slightly less favorable than that of stainless steel. For equal fuel exposure levels, 0.012 inch thick-walled Incoloy clad tubing is equivalent in fuel cycle costs to 0.015 inch thick-walled Type 304 stainless steel.[9] However, experience shows that extensive irradiation tests beyond the points at which stainless steel clad failures occurred must be made before the full capabilities of Incoloy clad fuel relative to stainless steel can be determined.

4.0 FABRICATION AND IRRADIATION HISTORY OF HPD FUEL ASSEMBLIES

4.1 Task 1A Fuel

A typical high power density VBWR fuel bundle is shown in Figure 1. All Task 1A fuel assemblies contain sintered UO_2 pellets clad with 304 stainless steel. The basic design features of the fuel are summarized in Table I.

The basic as-loaded fuel pellet-to-clad gap of 0.005 mils has been varied in 3C, 4C, group D, and group G to a range of between 0.002 and 0.003 inches by means of a light swage reduction pass. A description of the fabrication of Task 1A assemblies is presented in detail in GEAP-3609.[10]

4.2 Task 1B Fuel

The design criteria for the Task 1B fuel were basically the same as those used for the Task 1A fuel. The Task is mainly concerned with the development of improved, low cost fabrication processes and the performance in a reactor environment of fuel made by such processes. Several new structures for support and spacing of the fuel rods have been designed and tested under the program. The special powder fabrication processes such as tandem rolling, vibratory compaction, and swaging of various Task 1B fuel assemblies have been reported in topical and quarterly reports.[10,11,12,13,14,15,16,17,18,19,20] Design features of each of the Task 1B fuel assemblies as originally constituted are presented in Table II. Certain assemblies have been modified as a result of experimental needs responsive to the technical requirements of the program. These changes are shown in Table IV.

4.3 Fuel Irradiation and Failure History

The Task 1A fuel was loaded into the VBWR during September, 1960. No appreciable irradiation exposure occurred until January, 1961. The first Task 1B fuel (assemblies 1S and 2S) were loaded in the VBWR in April, 1961. The remaining Task 1B assemblies (through 10S) were loaded during 1961 and up to May, 1962.

All Task 1A assemblies operated satisfactorily until the early part of 1962. The operating history of all Task 1A assemblies is tabulated in Table III.

Table IV tabulates the operating history of all assemblies in the Task 1B group. During the months of February, April, July, August, and September, 1962, seven fuel assemblies were removed from VBWR because of indications of high activity release as measured by flux tilting and sipping techniques. Subsequent to this in the early part of 1963 through June additional failures have occurred in both Task 1A and 1B. Table V lists the core position at the time of failure and the approximate date of failure. Figure 2 shows in schematic form where the above failures occurred in-core.

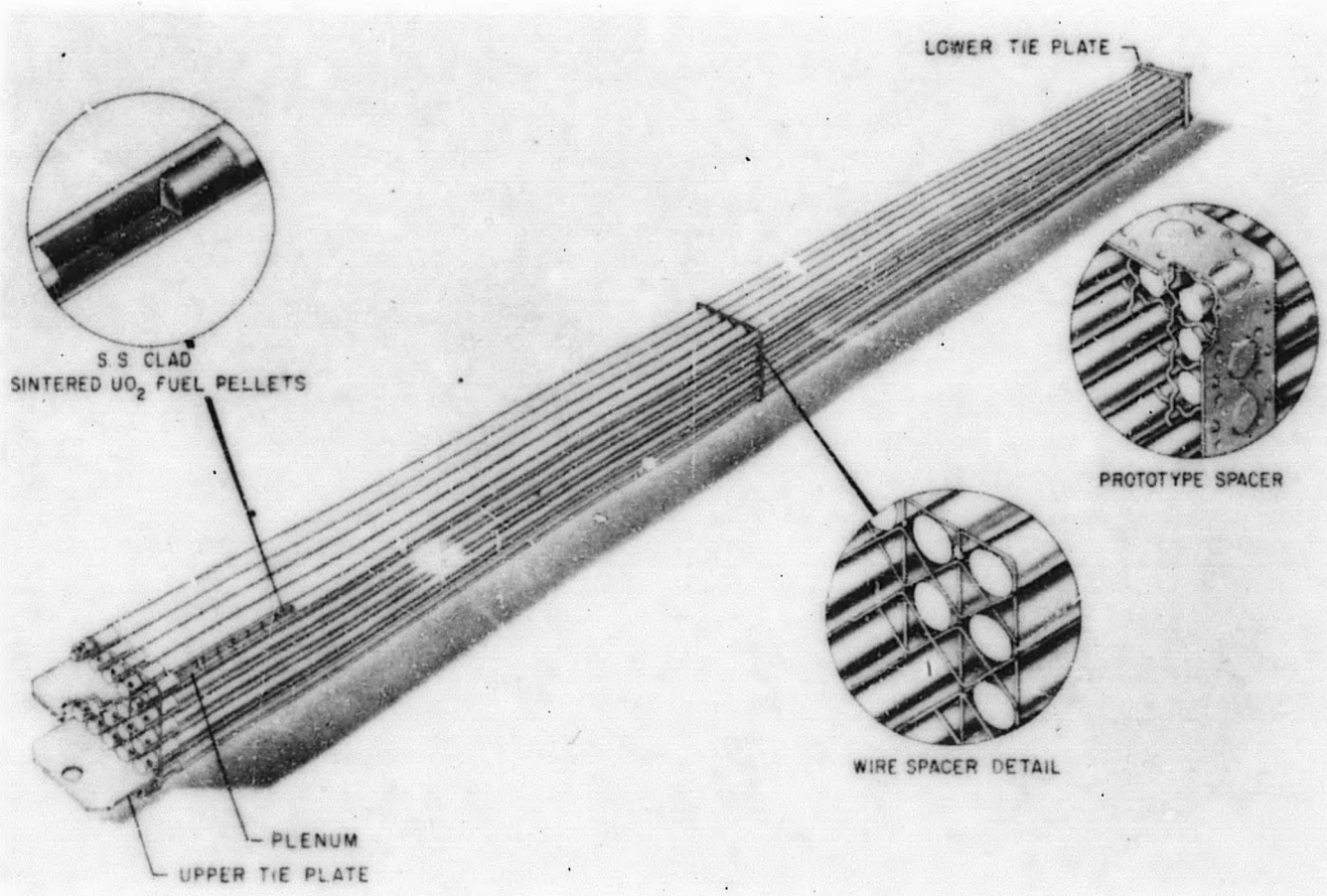

Figure 1. Typical High Power Density VBWR Fuel Assembly

TABLE I

TASK 1A FUEL DESIGN VARIABLES

Fuel Group	Rods Per Fuel Assembly	Total Number Fuel Rods	Clad OD Inches	Clad Thickness Inches	Clad Yield Strength psi[(a)]	Nominal UO_2-Clad Gap	Fabrication Process
A and B	16	64	0.420	0.020	38,000	0.005	Standard[(b)]
1C	25	25	0.417	0.017	38,000	0.005	Standard
2C	25	25	0.417	0.017	95,000	0.005	Standard
3C, 4C	25	50	0.410	0.017	95,000	0.003	Swaged[(c)]
D	25	100	0.398	0.012	94,000	0.002	Swaged
E	25	29	0.363	0.014	44,000	0.005	Standard
		120	0.363	0.014	90,000	0.005	Standard
F	25	49	0.363	0.014	90,000	0.005	Standard
G	25	20	0.360	0.014	44,000	0.002	Swaged
		80	0.360	0.014	90,000	0.002	Swaged

(a) The as-received room temperature yield strength of the tubing in all cases. The swaging process, imposing a very light reduction, makes very small changes in mechanical properties. Yield strengths of 38,000 and 44,000 represent commercially annealed material. Clad room temperature yield strengths of greater than the commercially annealed material are referred to as cold worked material.

(b) Standard pellet process uses centerless ground sintered UO_2 pellets encased in 304 stainless steel clad with welded end plugs. As-built-gap is determined by the pellet size and inside diameter of clad.

(c) Swaged fuel is essentially the same as the standard fuel, except that rotary swaging machines are used to vary the pellet-clad gap.

TABLE II

TASK 1B FUEL DESIGN VARIABLES

Fuel No.	Number Fuel Rods	Clad OD Inches	Clad Thickness Inches	Clad Yield Strength psi[a]	Fuel Fabrication Process[b]	UO_2 Density % of Theoretical
1S	23	0.400	0.012	94,000	Swaged Pellet[10]	95
	2	0.400	0.010	95,000	Vibratory Compacted Powder[13]	83
2S	13	0.400	0.016	95,000	Cold Swage Powder[12,14]	94
	12	0.400	0.010	95,000	Cold Swage Powder[12,14]	93
3S	21	0.400	0.016	90,000	Tandem Rolled Powder[11]	88-89
	4	0.400	0.012	80,000	Swaged Pellet (Corners)[1]	95
4S	16	0.360	0.014	40,000	Standard Pellet Fuel[1]	95
	9	0.360	0.014	80,000	Standard Pellet Fuel[1]	95
5S	10	0.400	0.008	95,000	Cold Swage Powder[3]	90-91
	5	0.400	0.010	95,000	Cold Swage Powder[3]	87-90
	10	0.400	0.016		Hot Swage Powder[3]	95
6S	12	0.400	0.010	45,000	Swaged Over Unground Pellets[1]	95
	13	0.390	0.008	52,000	Swaged Over Unground Pellets[1]	95
7S	12	0.400	0.012	80,000	Cold Swage Powder[3,5]	90-91
	13	0.400	0.016	95,000	Vibratory Compacted Powder[4]	86-88
8S	16	0.400	0.010	95,000	Cold Swage Powder[3,5]	91-92
9S	16	0.400	0.010	95,000	Cold Swage Powder[3,5]	91-92
10S	12	0.425	0.010	95,000	Cold Swage Powder[3 5]	89-92
	4	0.425	0.010	40,000	Swaged Pellet (Corners)[1]	95
11S	4	0.425	0.010	40,000	Swaged Pellet (Corners)[1]	95
	12	0.425	0.010	95,000	Swaged Powder[3,5]	89-91

(a) Cladding strength of 3-pass cold swaged fuel is raised during processing from about 45,000 to about 95,000 psi. All swaged powder fuel rods started with commercially annealed tubing.

(b) Numbers indicate references describing fuel processes in detail.

TABLE III
TASK 1A FUEL OPERATING HISTORY

Assembly Number	Average Bundle Exposure (MWD/t)[a]	Peak Bundle Exposure (MWD/t)[a]	Peak Heat Flux Btu/hr-ft²[b]	Maximum Average Power Density (KW/L)[e]	Peak Center Temperature (°F)[b]	Hours at Temperature	Hours Critical	Power Cycles[c]	Power Scrams[d]	Status	Illustration Showing Failure
1A	6650	10,600	361,000	80	2600	7220	9543	653	230	Operating	
2A	6650	10,600	358,000	79	2600	7220	9543	653	230	Operating	
1B	6800	10,850	400,000	88.9	2900	7220	9543	653	230	Operating	
2B	7000	11,250	417,000	92.9	2950	7220	9543	653	230	Operating	
1C	5200	8,300	381,000	109.7	2800	5200	6956	462	145	Operating	
2C	5900	9,400	400,000	108.2	2900	5827	7635	467	153	Operating	
3C	5000	8,050	400,000	103.9	2900	5235	7087	482	146	Operating	
4C	5650	9,000	393,000	109.3	2900	6256	8416	562	195	Operating	
1D	4950	7,900	400,000	110.4	2900	4912	7022	539	199	Failed	Figure 4
2D	4000	6,450	399,000	111.3	2900	3932	5844	439	180	Failed	Figure 5
3D	4300	6,850	440,000	109.2	3100	4252	6049	461	138	Failed	Figure 6
4D	1750	2,850	360,000	113.8	2600	1641	2840	190	80	Failed	
1E	6250	10,000	470,000	116.3	2850	4626	6666	513	192	Failed	Figure 7
2E	7900	12,700	470,000	113.9	2850	6401	8792	648	223	Failed	Figure 8
3E	8700	13,950	490,000	115.9	3100	6401	8792	648	223	Failed	Figure 9
4E	8400	13,500	462,000	109.8	3000	6482	8801	601	215	Failed	Figure 10
5E	8050	12,850	454,000	111.6	3000	6401	8792	648	223	Failed	
6E	7650	12,250	471,000	117.7	3000	5931	7314	486	164	Failed	Figure 11
1F	7450	11,900	480,000	116.2	3050	5574	7526	501	180	Operating	
2F	6900	11,050	460,000	111.8	3000	5447	6813	484	163	Failed	
1G	6000	9,600	480,000	118.8	3050	4716	6803	523	196	Failed	Figure 12
2G	5600	9,000	488,000	120.7	3050	4228	6175	467	182	Failed	Figure 13
3G	7250	11,600	500,000	120.5	3100	5573	7863	618	211	Failed	Figure 14
4G	8100	12,950	488,000	119.8	3050	5983	8306	625	218	Failed	

(a) In the case of those assemblies still operating, exposures are as of June 30, 1963.

(b) Maximum experienced during lifetime.

(c) A power change from below 4 MWt to above 4 MWt and back is considered to be one power cycle.

(d) Any scram occurring above 5 MWt.

(e) Average for bundle.

TABLE IV

TASK 1B FUEL OPERATING HISTORY

Assembly Number	Average Bundle Exposure[a] (MWD/t)	Peak Bundle Exposure[a] (MWD/t)	Peak Heat Flux[b] (Btu/hr-ft^2)	Maximum Average[f] Power Density (KW/L)	Peak Center[b] Temperature (°F)	Hours at Temperature	Hours Critical	Power[d] Cycles	Power[e] Scrams	Status
1S	1800	2851	380,000	86	2800	1958	2794	236	101	Reconstituted, see below
1SM-1	3800	6100	460,000	95.2	3150	4408	5604	456	135	13-7S vibratory compacted rods
	4500	7182	380,000	100	2700	4691	6039	486	156	8-3S tandem rolled rods
	1800	2850	380,000	86	2800	1958	2794	236	101	4-1S vibratory compacted rods
2S	4500	7100	385,000	92.7	2800	5271	6806	530	173	Failed, (2 rods failed, Figure 15)
3S	4500	7180	380,000	100	2800	4691	6039	486	156	Failed, (4 corner rods failed, Figures 16, 17, 18, 19.)
4S	6200	9900	490,000	106	3100	4800	5900	407	119	Operating
5S	3960	6340	425,000	109.2	3000	4454	5511	404	113	Failed (suspect)
6S	5270	8440	410,000	106.7	3000	5469	6917	504	168	Failed (two rods failed)(Figures 20,21)
7S	3800	6100	460,000	95.2	3200	4408	5604	456	135	Failed, 13 sound vibratory compacted rods placed in 1SM-1 for continued irradiation (failure based on visual and ultrasonic results)
8S	3524	5638	527,000	101	3500	2741	3363	265	50	Failed (suspect)
9S	4100	6546	490,000	120	3300	3560	4213	270	57	Bundle operating
10S	2120	3390	450,000	93	3200	2173	2617	181	41	Failed (suspect)
11S	--	--	---	--	--	--	--	--	--	Proposed reconstitution from Task 1A "E" assembly cold worked rods
(c) 12S	7746	11,600	490,000	117.7	3100	6100	8200	590	207	Reconstituted from Task 1A "E" assembly annealed rods.

(a) As of June 30, 1963
(b) Maximum experienced during lifetime
(c) Average of all "E" series rods placed in assembly
(d) A power change from below 4 MWt to above 4 MWt and back is considered to be one power cycle.
(e) Any scram occurring above 5 MWt.
(f) Average for bundle.

TABLE V
CORE LOCATIONS AT TIME OF FAILURE

Assembly No.	Core Position	Run No.	Date of Failure*
1D	H-9	151	8/ /62
2D	H-9	147	4/29/62
3D	M-9	154	3/ 5/63
4D	K-8	146	4/20/62
1E	G-8	149	7/ 8/62
2E	F-9	158	4/25/63
3E	H-7	158	4/25/63
4E	K-9	159	5/12/63
5E	F-7	158	4/25/63
6E	L-9	159	6/ 2/63
2F	L-10	158	4/25/63
1G	K-9	150	7/24/62
2G	K-8	148	6/12/62
3G	K-9	154	3/ 5/63
4G	L-8	155	3/23/63
2S	H-11	154	3/ 5/63
3S	G-9	155	9/62 and 3/23/63***
5S**	J-9	158	4/25/63
6S	H-11	156	4/ 4/63
7S	E-10	158	4/25/63
8S**	K-5	158	4/25/63
10S**	K-12	158	4/25/63

* End-of-run date
** "Suspect" failures have been proposed for re-insertion in VBWR.
*** Following the initial failure of one corner rod the assembly was reinserted in the VBWR (after removal of the failed rod).

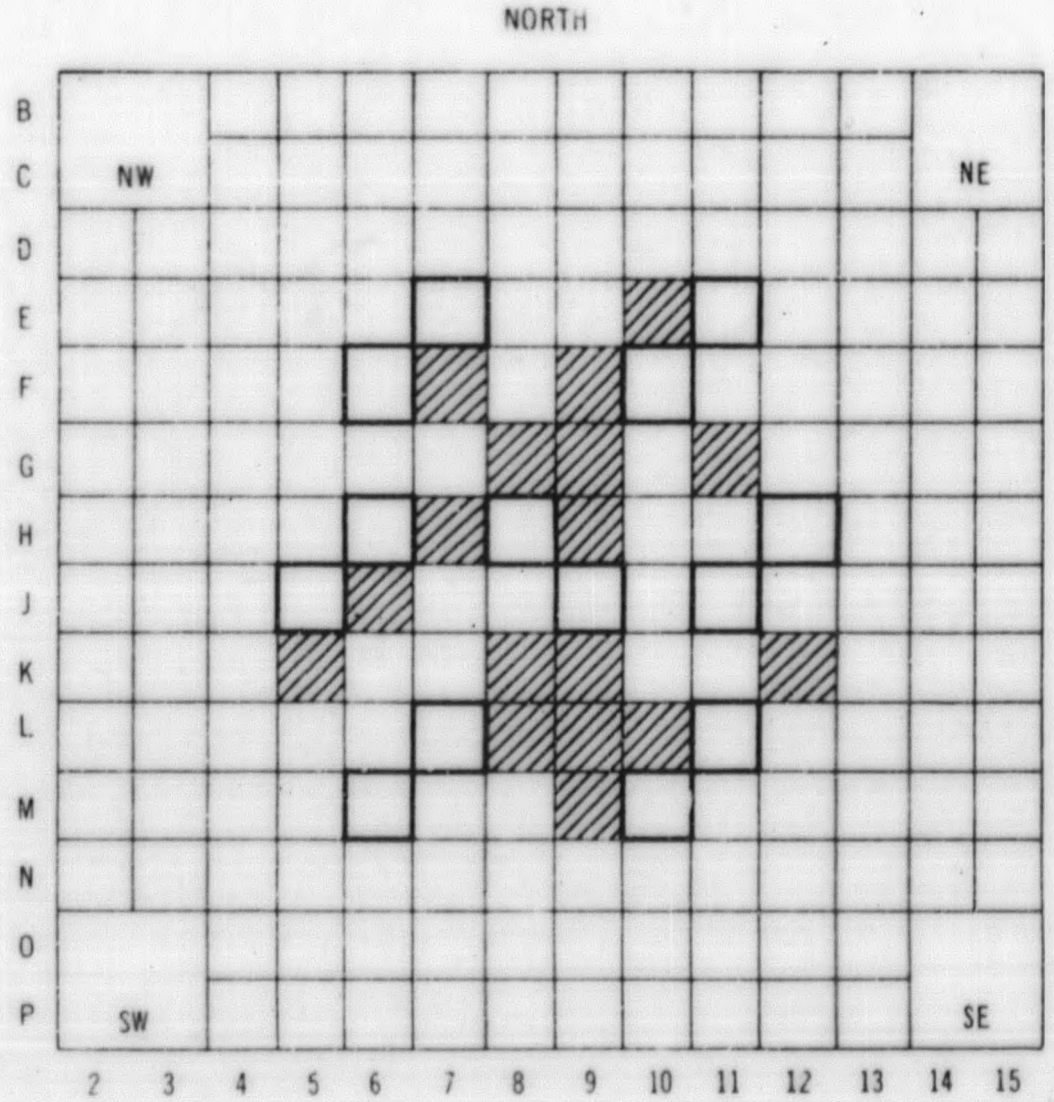

Figure 2. VBWR Core Plot; Locations Where Failures Have Occurred

5.0 FAILURE EXAMINATION AND RESULTS

5.1 Failure Detection Methods and Examination

Failure of fuel in the VBWR is first shown by an increase in both the air ejector off-gas activity level and the reactor water iodine activity. The off-gas is monitored continuously and the reactor water gross iodine activity level is measured daily. Several methods are used to locate a failed fuel assembly: (1) Flux tilting--peaking or depressing selected areas of the core by control rod manipulation produces a corresponding change in the off-gas release rate and indicates the general core location of the failed fuel; (2) The multitube in-core sampler--this unit enables one to measure the fission gas release rates from individual fuel assemblies while the reactor is at power. The equipment is arranged for sampling ten assemblies and normally these are selected and inserted under the sampler if they are "suspect" leakers or for any reason are considered vulnerable to failure; (3) Sipping[22] -- suspect assemblies are isolated in a small volume of coolant and the amount of active iodine contamination of this coolant measured and compared to background. A tabulation of such data has been selected as illustrative and is presented in Table VI for failed and nonfailed assemblies. Subsequent to the sipping a suspect assembly is visually scanned either in the VBWR pool with an underwater Lerme periscope or in the RML by means of a Kollmorgen cell periscope. Augmenting visual checks (especially in those cases involving very small cracks) ultrasonic examinations are used in the pool and in the cells.

Figure 3 gives the identification system and permits location of failed fuel rods within an assembly. To show the visually detectable rod failures, the photographs in Figures 4 through 21 show the condition of the failures upon visual examination.

In later sections the experimental observations and data covering those assemblies subjected to detailed hot cell examinations are reported.

Examination of Figures 4 through 21 yields the following observations:

1. With the exception of HPD 4E and 6S, all failures have occurred in cold worked material.
2. With the exception of HPD 4E, all failures can be observed as primarily longitudinal in nature.
3. All failures have occurred in the peak heat flux region of the rod.
4. Even where the UO_2 fuel is exposed to the reactor environment, very small loss of fuel material has occurred.
5. With the exception of HPD 2S and 7S (powder fuel) all failures have occurred in pellet fuel. The failures of rods in HPD Assembly 2S are reported in detail separately.[21]

TABLE VI

REPRESENTATIVE SIPPING RESULTS[a]

Assembly	Ratio I-131/Background	Ratio I-132/Background	Indication of:
1A[b]	0.5	1.2	No leak
2A	0.5	1.2	No leak
1C	1.1	---	No leak
2C	1.4	16.2	No leak
2E	69.5	---	Failure
3E	105	44	Failure
4E	7.7	23.1	Possible leak
5E	3.7	15.0	Possible leak
6E	171	156	Failure
1F	1.4	0.6	No leak
2F	27.1	122	Failure
5S	1.30	25.6	Possible leak
6S	7.8	43.2	Failure
7S	1	---	No leak
8S	26	30	Possible leak
9S	1.7	13.3	No leak
10S	0.9	20.2	Possible leak

(a) All samples were taken following Run 158 (May 12, 1963) except:
4E, 6E - Sampled at the end of Run 159 (June 2, 1963)
6S Sampled at the end of Run 156 (April 5, 1963)

(b) Assemblies 1A and 2A are fuel followers and were sampled while still in core without the use of sipper cans.

AS LOADED CONFIGURATION:

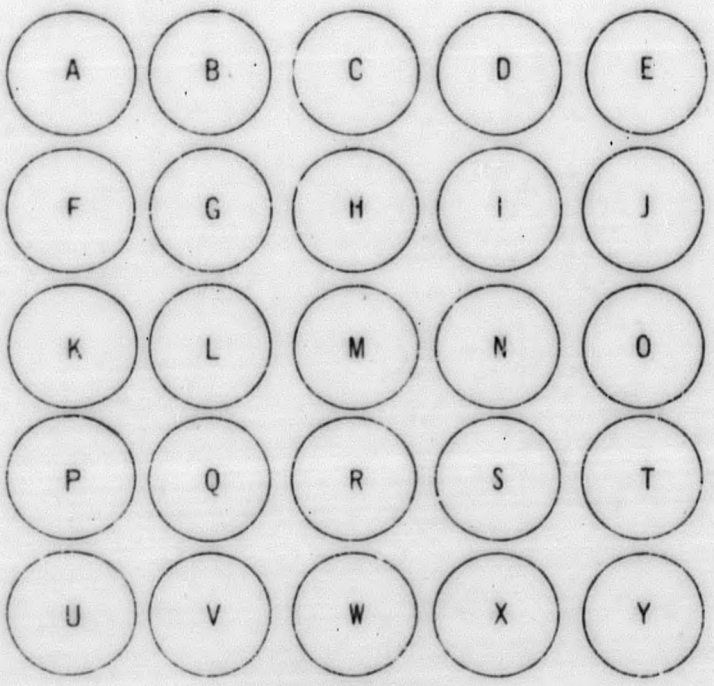

Figure 3 Location of Individual Fuel Rods Within An Assembly

Longitudinal cracking observed in failed rod.

0.398 in. × 0.012 in. 304 SS clad UO_2 0.002 in. nominal gap
Initial clad condition: Cold worked 94,000 psi Y.S.
Failure location: Peak heat flux region
Exposure at failure location: 7900 MWD/t
Heat Flux at failure location: 400,000 Btu/hr-ft^2

No detailed examination performed.

Figure 4. HPD 1D - Rod E Service Failure

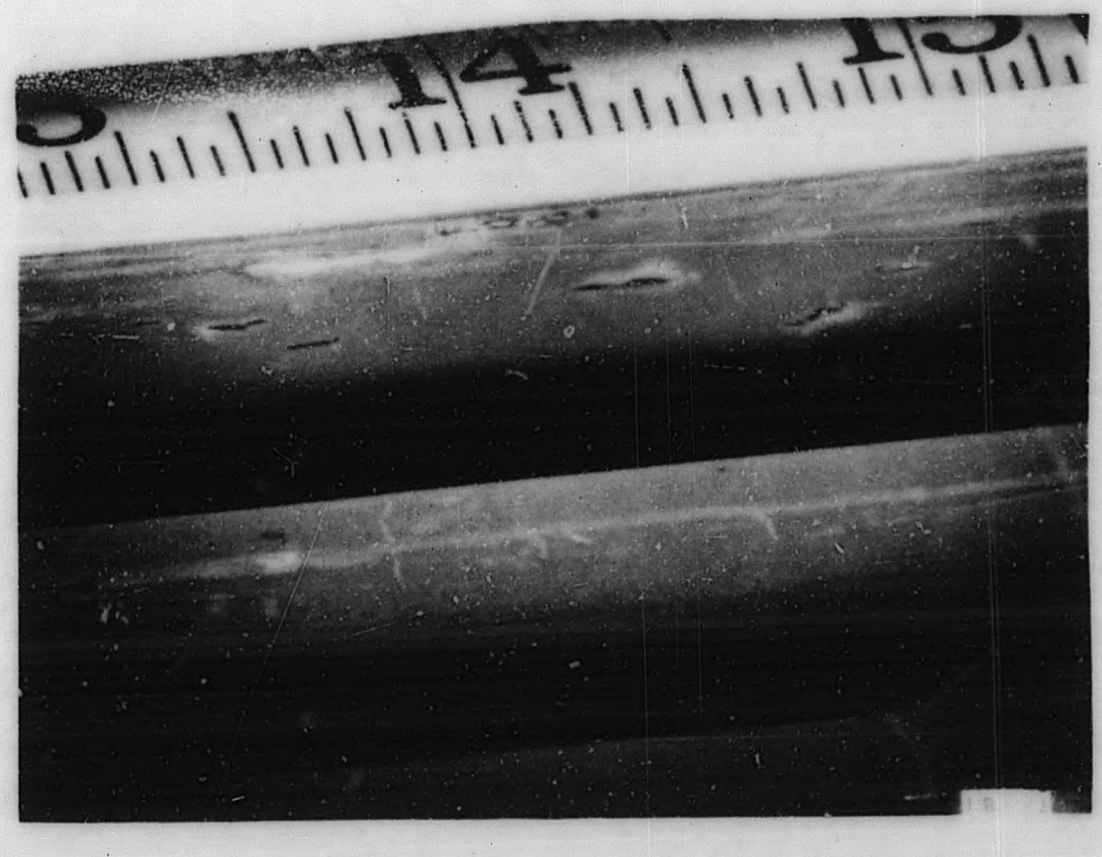

Short longitudinal cracks in fuel clad

0.398 in. × 0.012 in. 304 SS clad UO_2 0.002 in. nominal gap
Initial clad condition: Cold worked, 94,000 psi Y.S.
Failure location: Peak heat flux region
Exposure at failure location: 6400 MWD/t
Heat flux at failure location: 399,000 Btu/hr-ft^2

Detailed examination performed.

Figure 5. HPD 2D - Rod A Service Failure

Failure occurred 8½ to 9½ inches from bottom end.

0.398 in. × 0.012 in. 304 SS clad UO_2
0.002 in. nominal gap
Initial clad condition: Cold worked, 94,000 psi Y.S.
Failure location: Peak heat flux region
Exposure at failure location: 6900 MWD/t
Heat Flux at failure location: 440,000 Btu/hr-ft^2

No detailed examination performed.

Figure 6. HPD 3D - Rod V Service Failure

Failure occurred 9½ to 10½ inches from bottom.

0.363 × 0.014 304 SS clad UO_2
0.005 inch nominal gap
Initial clad condition: Cold worked, 90,000 psi Y.S.
Failure location: Peak heat flux region
Exposure at failure location: 10,000 MWD/t
Heat Flux at failure location: 470,000 Btu/hr-ft^2

Detailed examination performed.

Figure 7. HPD 1E - Rod E Service Failure

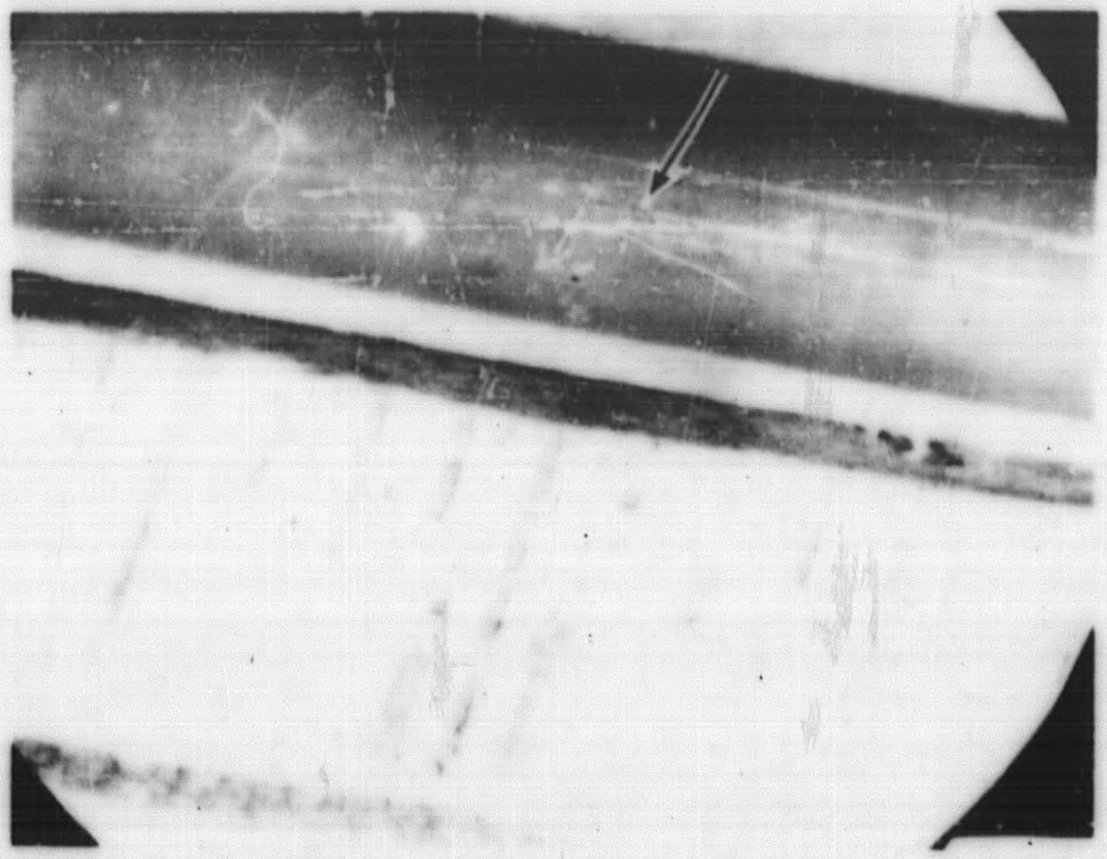

Longitudinal crack 11 inches from bottom.

0.363 × 0.014 304 SS clad UO_2
0.005 inch nominal gap
Initial clad condition: Cold worked, 90,000 psi Y.S.
Failure location: Peak heat flux region
Exposure at failure location: 12,700 MWD/t
Heat flux at failure location: 470,000 Btu/hr-ft^2

Detailed examination planned.

Figure 8. HPD 2E - Rod O Service Failure

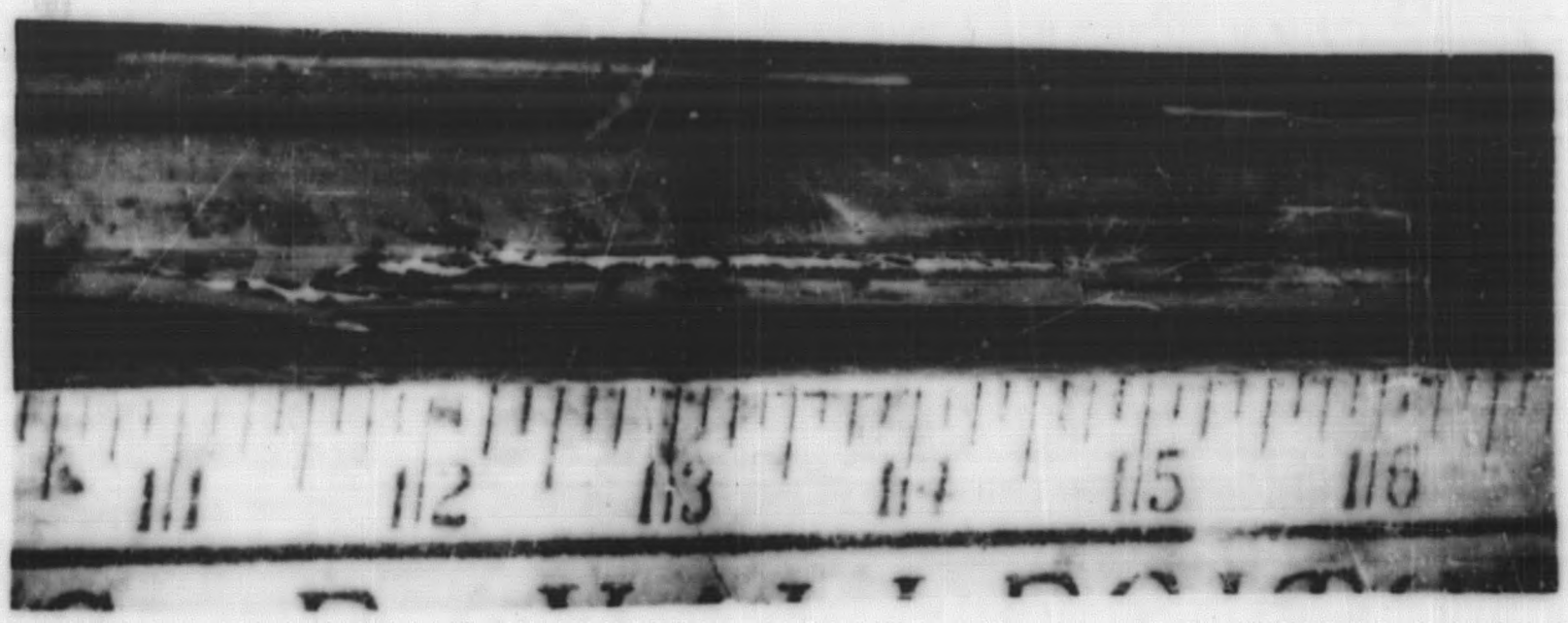

Gross failure 10½ to 16 inches from bottom.

0.363 in. × 0.014 in. 304 SS clad UO_2
0.005 inch nominal gap
Initial clad condition: Cold worked 90,000 psi Y.S.
Failure location: Peak heat flux region
Exposure at failure location: 13,900 MWD/t
Heat flux at failure location: 490,000 Btu/hr-ft^2

No detailed examination performed.

Figure 9. HPD 3E - Rod X Service Failure

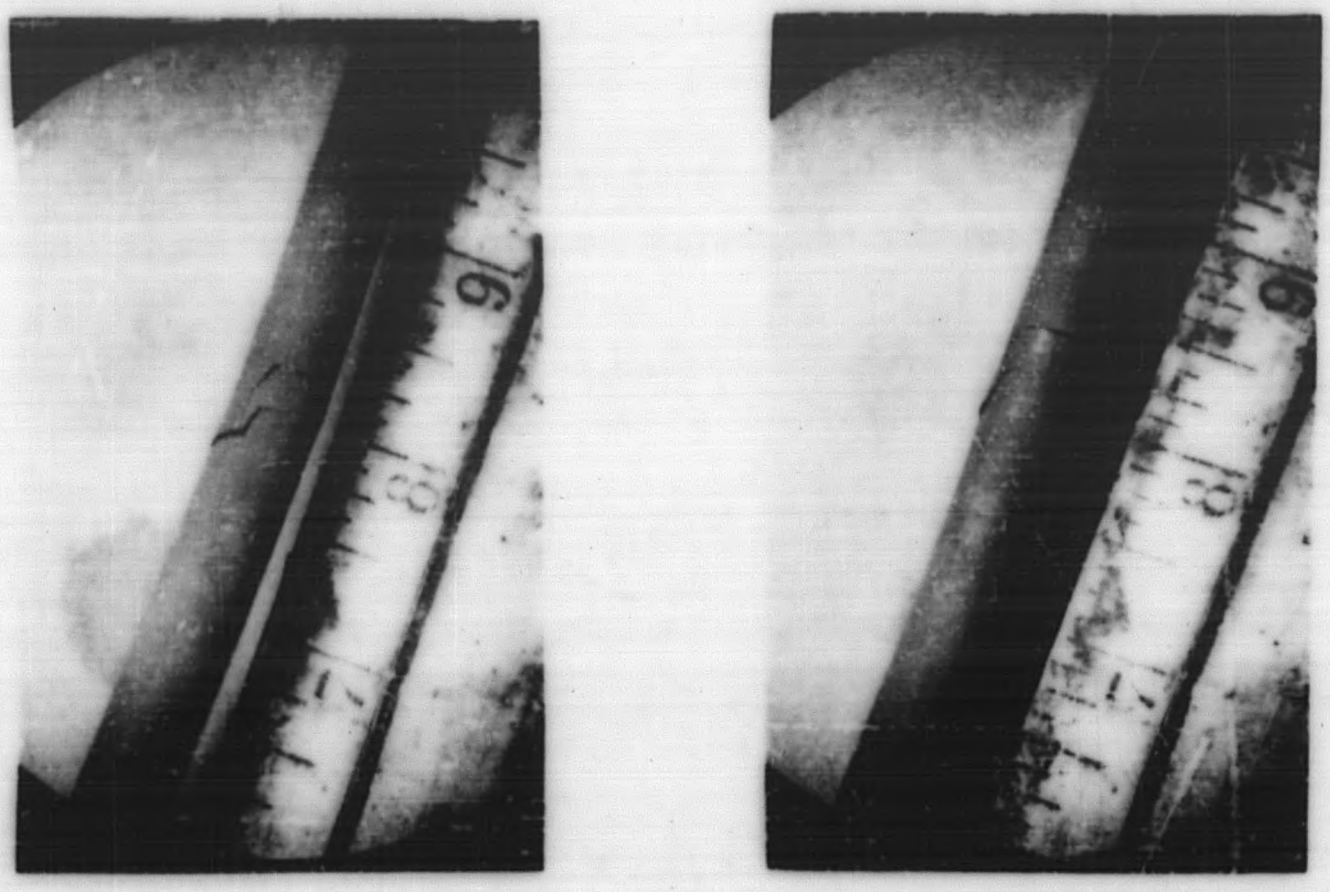

(a) 0°

(b) 90°

First complete circumferential cracking found in HPD program.

0.363 in. × 0.014 in. 304 SS clad UO_2
0.005 inch nominal gap
Initial clad condition: Annealed 44,000 psi Y.S.
Failure location: Peak heat flux region
Exposure at failure location: 13,500 MWD/t
Heat flux at failure location: 460,000 Btu/hr-ft^2

See Appendix A for additional views and photomicrographs.

Figure 10. HPD 4E - Rod C Service Failure

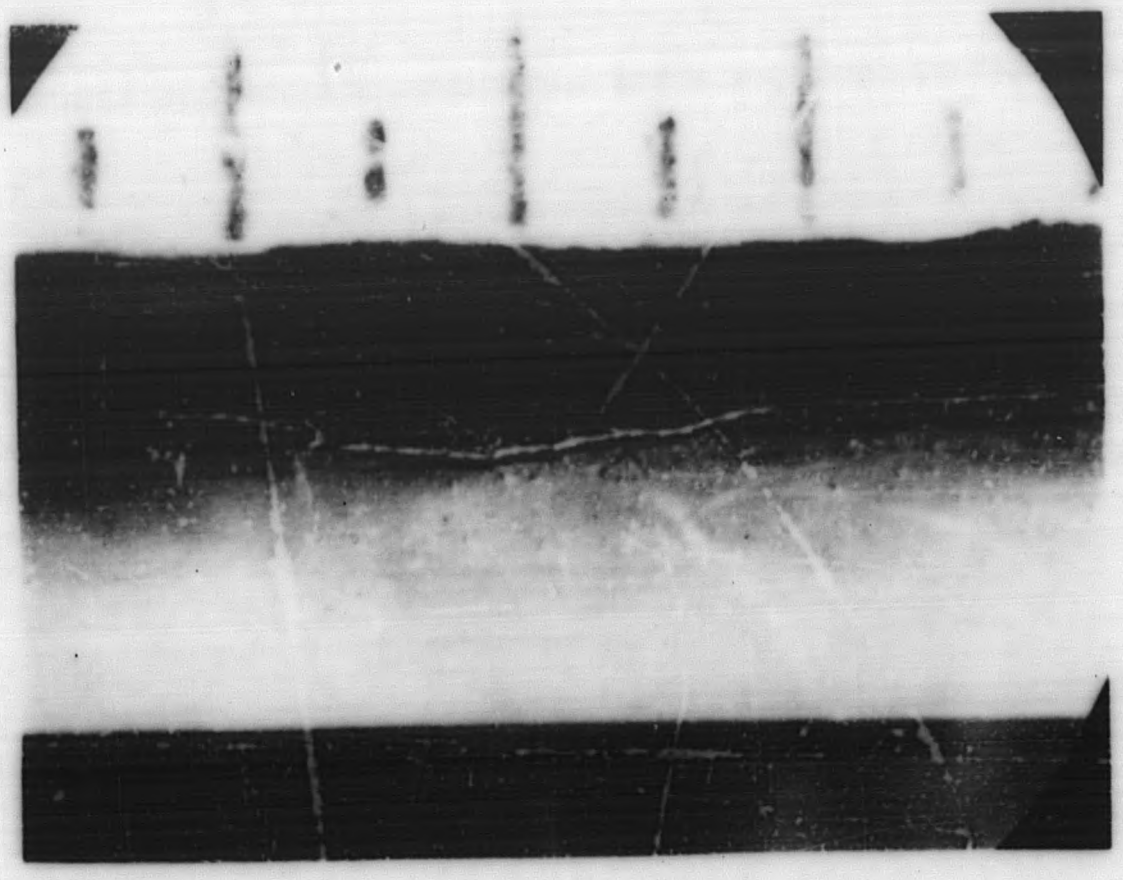

0.363 in. x 0.014 in. 304 SS clad UO_2
0.005 inch nominal gap
Initial clad condition: Cold worked 90,000 psi Y.S.
Failure location: Peak heat flux region
Exposure at failure location: 12,200 MWD/t
Heat flux at failure location: 470,000 Btu/hr-ft^2

No detailed examination performed.

Figure 11. HPD 6E - Rod A Service Failure

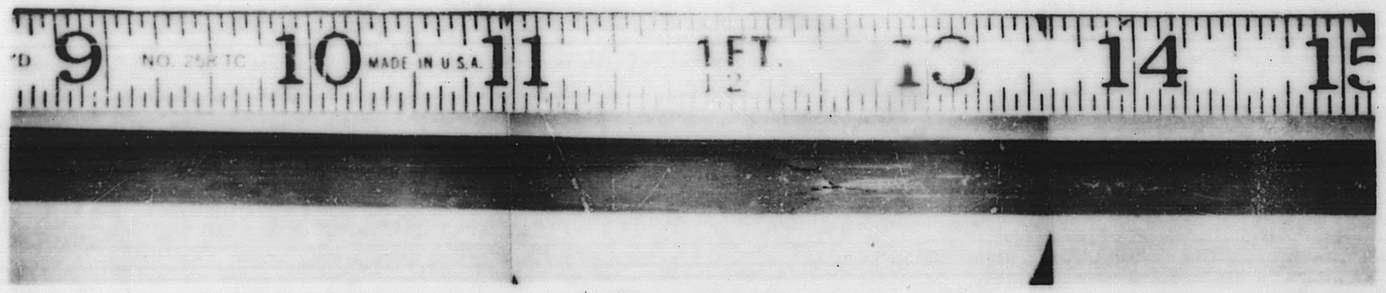

Longitudinal Cracking

0.360 × 0.014 304 SS clad UO_2
0.002 inch nominal gap
Initial clad condition: Cold worked 90,000 psi Y.S.
Failure location: Peak heat flux region
Exposure at failure location: 9600 MWD/t
Heat flux at failure location: 480,000 Btu/hr-ft^2

See Figures 24-34 for more pictures and metallography of 1G.

Figure 12. HPD 1G - Rod R Service Failure

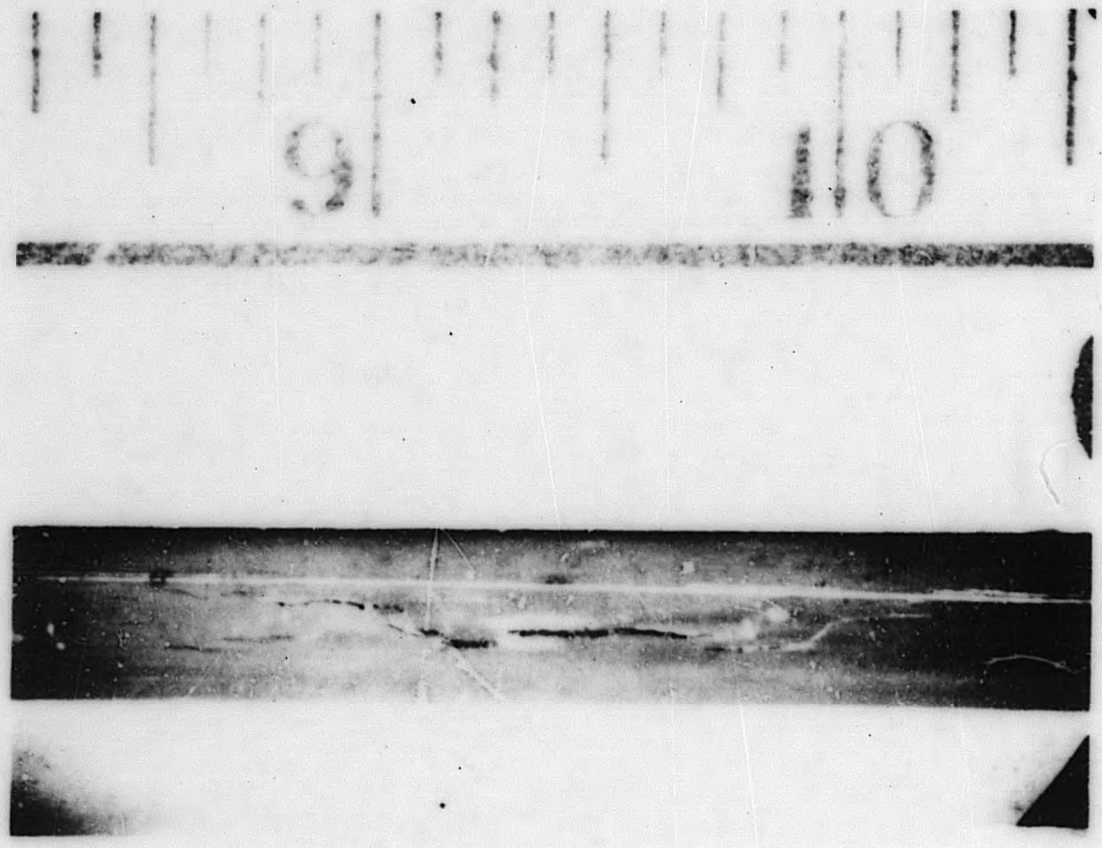

Irregular longitudinal crack in peak flux region.

0.360 in. × 0.014 in. 304 SS clad UO_2
0.002 inch nominal gap.
Initial clad condition: Cold worked, 90,000 psi Y.S.
Failure location: Peak heat flux region
Exposure at failure location: 9000 MWD/t
Heat flux at failure location: 480,000 Btu/hr-ft^2

Detailed examination performed.

Figure 13. HPD 2G - Rod G Service Failure

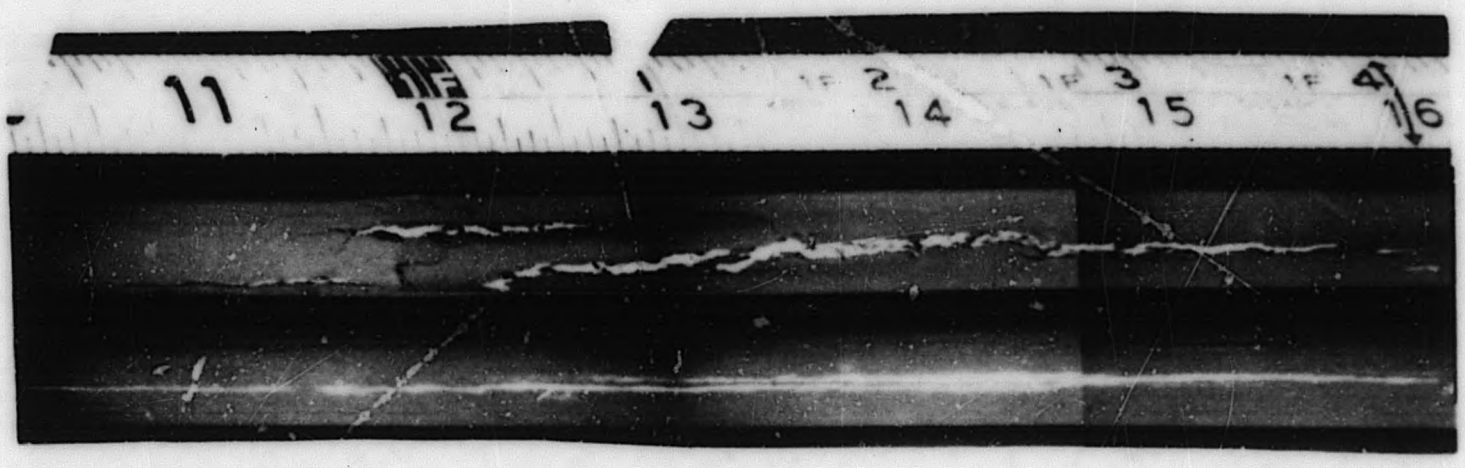

a. HPD 3G - Rod B Service Failure

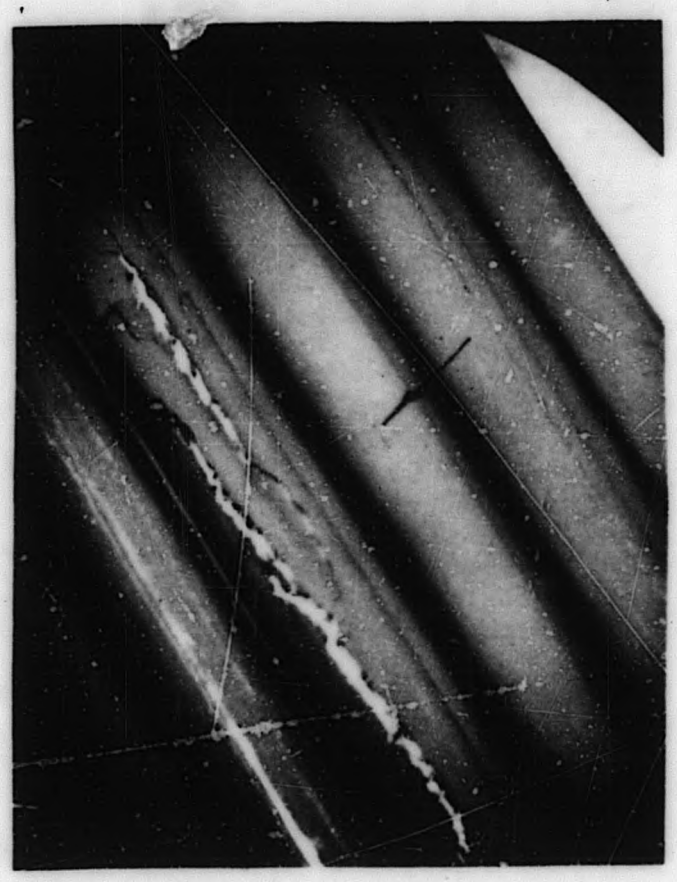

b. HPD 3G - Rod C Service Failure

c. HPD 3G - Rod E Service Failure

0.360 in. × 0.014 304 SS cladding

0.002 nominal gap

Initial clad condition: Cold worked, 90,000 psi Y.S.
Failure Location: Peak Flux Region
Exposure at failure location: 11,600 MWD/t
Heat flux at failure locations: 500,000 Btu/hr-ft^2

No detailed examination performed.

Figure 14. HPD 3G - Rods B, C and E Service Failure

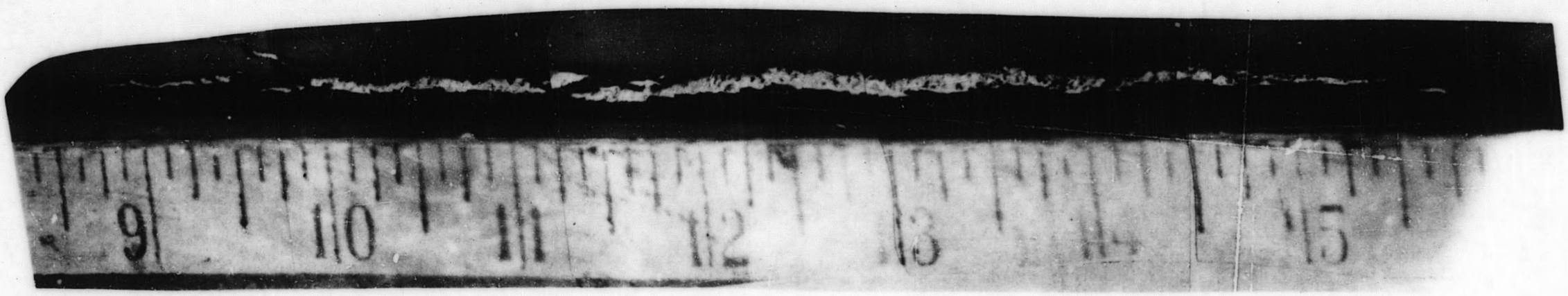

Longitudinal split in Rod Number 437, Rod I Assembly HPD-2S. The cladding is Type 304 stainless steel, 0.011 inch thick. The fuel is fused uranium dioxide swaged to a density of 93±1 percent of theoretical. Only a small amount of fuel was lost to the reactor coolant.

Figure 15. HPD 2S - Rod I Service Failure

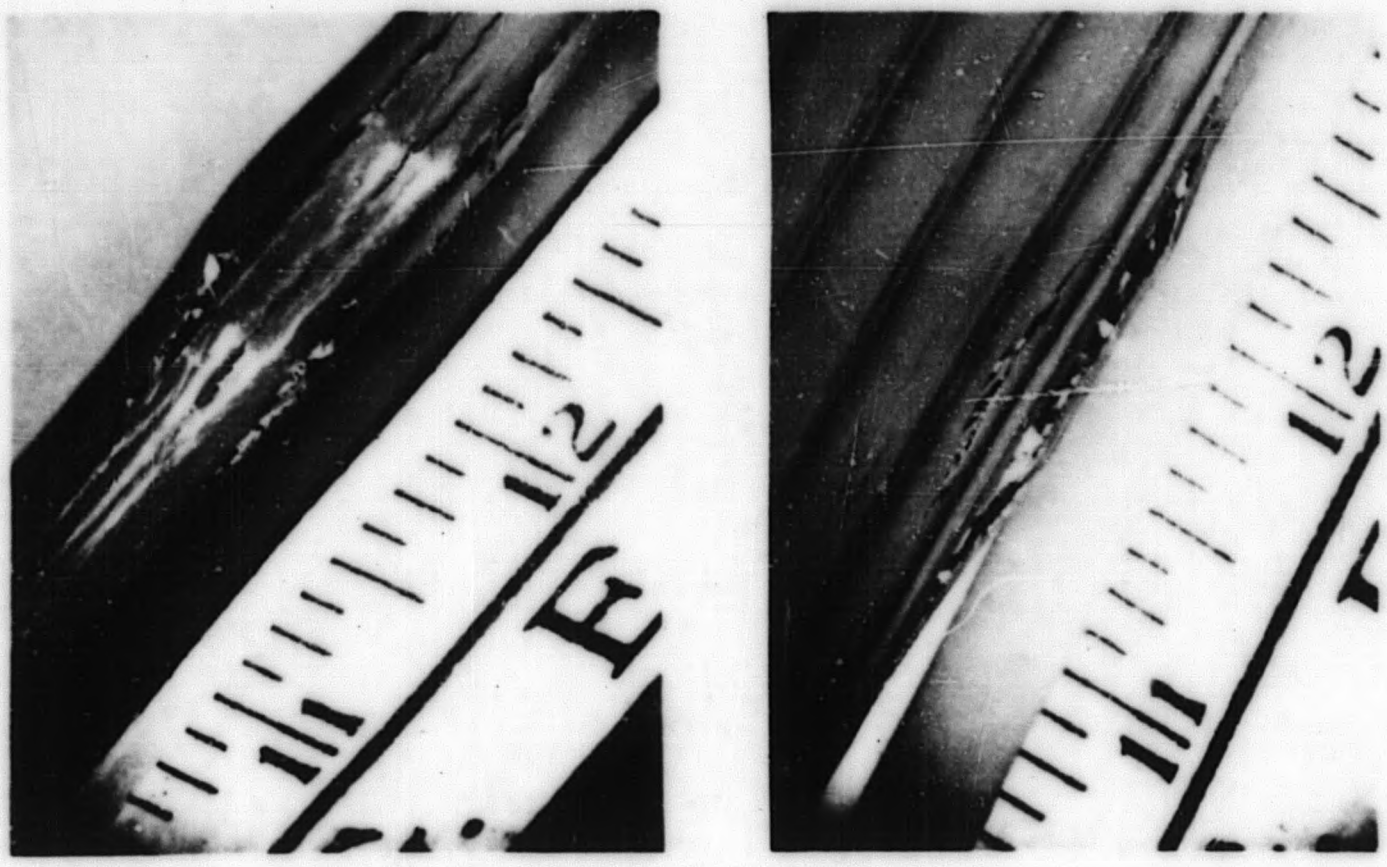

(a) 0°

(b) 90°

First failure experienced in bundle - Rod identical to those in "D" series assemblies of Task 1A.

0.400 in. × 0.012 in. 304 SS clad UO_2
0.002 in. nominal gap
Initial clad condition: Cold worked, 80,000 psi Y.S.
Failure location: Peak heat flux region
Exposure at failure location: 6200 MWD/t
Heat flux at failure location: 380,000 Btu/hr-ft^2

Detailed examination performed.

Figure 16. HPD 3S - Rod E Service Failure

Longitudinal Cracking

0.400 in. × 0.012 in. 304 SS clad UO_2
0.002 nominal gap
Initial clad condition: Cold worked, 80,000 psi Y.S.
Failure location: Peak heat flux region
Exposure at failure location: 7200 MWD/t
Heat flux at failure location: 380,000 Btu/hr-ft^2

Detailed examination performed.

Figure 17. HPD 3S - Rod A Service Failure

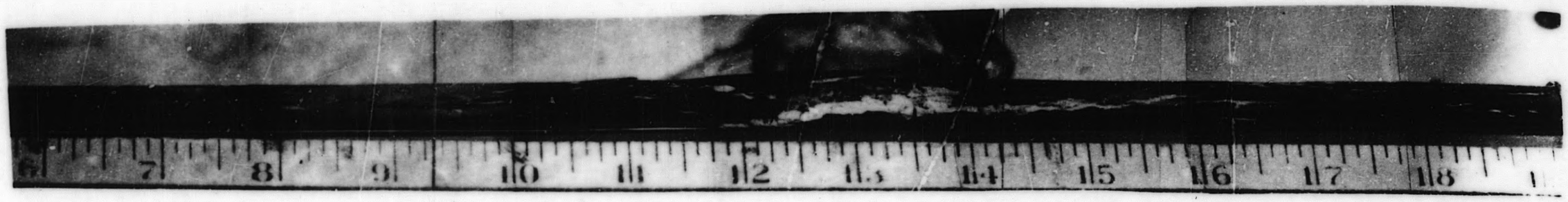

Longitudinal Cracking

0.400 in. × 0.012 in. 304 SS clad UO_2
0.002 nominal gap
Initial clad condition: Cold worked, 80,000 psi Y.S.
Failure location: Peak heat flux region
Exposure at failure location: 7200 MWD/t
Heat flux at failure location: 380,000 Btu/hr-ft^2

No detailed examination performed.

Figure 18. HPD 3S - Rod U Service Failure

Longitudinal Cracking

0.400 in. × 0.012 in. 304 SS clad UO_2
0.002 nominal gap
Initial clad condition: Cold worked, 80,000 psi Y.S.
Failure location: Peak heat flux region
Exposure at failure location: 7200 MWD/t
Heat flux at failure location: 380,000 Btu/hr-ft^2

No detailed examination performed.

Figure 19. HPD 3S - Rod Y Service Failure

0.390 in. × 0.008 in. 304 SS clad UO_2 unground pellets
0 to 0.002 inch nominal gap
Initial clad condition: Cold worked, 52,000 psi Y. S.
Failure location: Peak heat flux region
Exposures in failure location: 8450 MWD/t
Heat flux in failure location: 410,000 Btu/hr-ft^2

Photo taken with periscope in VBWR Pool - no detailed examination planned.

Figure 20. HPD 6S - Rod B Service Failure

0.390 in. × 0.008 in. 304 SS clad UO_2 unground pellets
0 to 0.002 inch nominal gap
Initial clad condition: Cold worked, 52,000 psi Y.S.
Failure location: Peak heat flux region
Exposures in failure location: 8450 MWD/t
Heat flux in failure location: 410,000 Btu/hr-ft^2

Photo taken with periscope in VBWR Pool - no detailed examination planned.

Figure 21. HPD 6S - Rod D Service Failure

Several assemblies suspected to contain rods with leaks are not included in the pictorial summary. These have not been finally verified as failures but have been classified as "suspect failures" on the basis of radiochemical evidence as presented in Table VI. These assemblies, 5S, 8S and 10S, will be reinserted (probably one at a time) in the VBWR under the multi-tube sampler during the latter portion of 1963.

5.2 Detailed Fuel Failure Examinations

The extent of post-irradiation examination performed on fuel assemblies containing failed fuel rods has necessarily varied. In general, examination was more intense on those assemblies first experiencing fuel rod service failures. In addition, the macroscopic appearance of the failure, and the type of rod failed, determined to a great extent the degree of detail desired in the examination. For example, the recent annealed rod failure (rod C from assembly 4E - as the first of a kind) is being examined in detail. A summary of the post-irradiation examination performed on each fuel assembly and failed rods is presented in Table VII.

5.2.1 Ultrasonic Testing

The use of ultrasonic testing techniques in locating fuel cladding defects has been very effective. Its application has been introduced successfully at the VBWR fuel storage pool and in RML cells as a part of the HPD program.

Work has been done at the VBWR storage pool in inspecting the outer segments of fuel elements for longitudinally oriented defects. Test equipment used was a focused lithium sulphate 10 mc transducer on 30 feet of RG 59/U cable driven by a high voltage spike pulser, an M630 wide band amplifier, and a Tektronix 3 21 oscilloscope. A problem has been the reliability of the information received from the inspection. In several cases defective rods were discovered when bundles were visually scanned at RML subsequent to ultrasonic testing. Equipment improvements are in progress for pool work.

The in-cell testing at RML thus far has been more reliable at finding "hard-to-see" flaws than the pool inspections. Sensitivity of the equipment is entirely comparable to a similar test run outside of the cell. In several cases the testing revealed fine hairline cracks not readily visible. Upon close visual examination in the areas of strong ultrasonic signals, these cracks were identified positively.

Figure 22 is a photograph of the in-cell test set-up as used in the HPD program.

Representative data obtained by ultrasonic testing in RML is presented in Table VIII. This work is conducted on individual rods mounted for rotation in a manner essentially duplicating the routine testing of as-received tubing in the APED Manufacturing Section.

TABLE VII

SUMMARY OF HPD PROGRAM

POST-IRRADIATION EXAMINATIONS

Assembly Number	Visual Examination	Disassembly	Ultrasonic Inspection	Dimensional Measurements	Gamma Scan	Fission Gas Analysis	Burnup	Crud Analysis	Metallography	Tensile Tests	Burst Test	Microhardness	Electron Microscopy	Rods Examined Metallographically
1D	X													
2D	X	X	X	X	X	X	X	X	X			X		A, E, V
3D	X													
4D	X													
1E	X	X	X	X	X		X	X	X			X		E
2E	*	*	*	*	*		*					*		E
3E	X													
4E	*	*	*	*	*		*		*			*		C, B
5E	X													
6E	X													
2F	X													
1G	X	X	X	X	X	X	X		X	X	X	X	*	B, Q, R, W
2G	X	X	X	X	X	X	X	X	X			X		B, G
3G	X													
4G	X													
2S	X	X	X	X	X	X	X		X			X		I
3S	X	X		X	X		X		X			X		E
5S	X													
6S	X													
7S	X													
8S	X													
10S	X													

* Examinations of assemblies are in progress

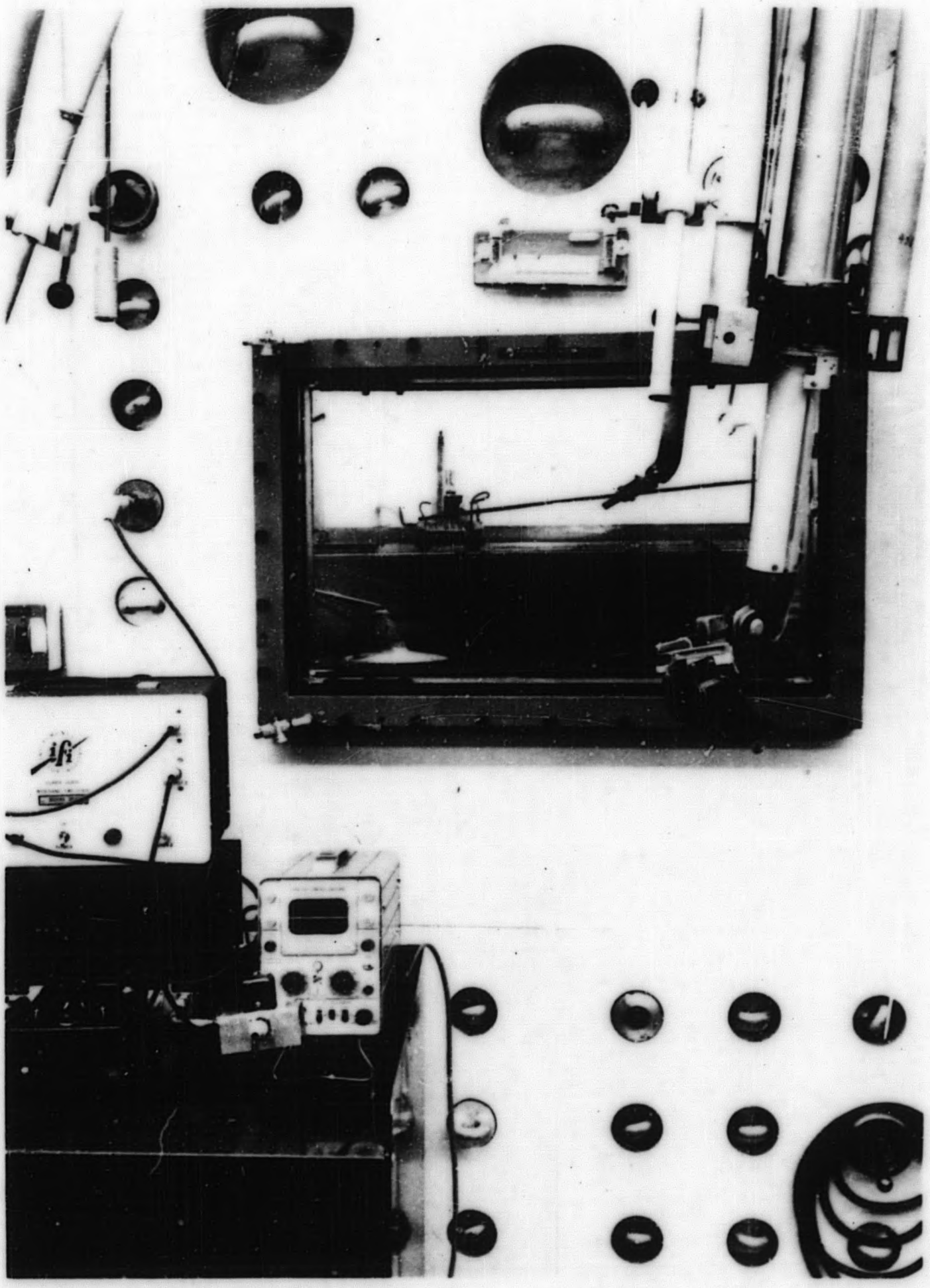

Figure 22. In-Cell Ultrasonic Testing Setup

TABLE VIII

ULTRASONIC RESULTS vs. VISUAL SCANS CONDUCTED AT RML

Bundle Rod [a]	Reflection Locations (Inches from Top)	Signal Strength [b]	Verification (Visual or Metallurgical)
1G-R	28, 24, 22, 19, 11	L-S	Visual and destructive examination
1G-D	28, 13, 10, 9	L-S	None
1G-N	29, 22, 18, 17, 14	S	None
1G-Q	28, 24, 19, 13, 11, 7	SML	Destructive examination
1G-C	7, 8, 12, 19	M	None
1G-L	28	S	None
1G-W	10	M	None
1G-V	6	S	None
1G-F	24, 8	S	None
1G-A	15	S	None
1G-Y	6, 8	M	None
1G-E	22	S	None
2G-G	20 $\frac{1}{2}$, 19, 12, 11, 9 $\frac{1}{2}$, 8, 7 $\frac{1}{2}$, 4 $\frac{1}{2}$, 3	L	Destructive examination
2G-N	30 $\frac{1}{2}$, 29, 28, 27, 21, 12, 9	ML	Visual at 28 inches

(a) All rods in each assembly were checked but those rods not indicating any signal at all are deleted from the table. In all, 100 segments were checked from this group.

(b) S - Small signal (10 percent of wall or less)
M - Medium signal (> 10 percent < 50 percent of wall)
L - Large signal (>50 percent of wall)

5.2.2 Dimensional Measurements

The examination of fuel rods for both diametral and longitudinal growth consists primarily of:

1. The measurement of the OD of the rods along the full length every two (2) inches at 0° and 90°.
2. A longitudinal check of length measured from the shoulders of the end plugs.

Post-irradiation measurement can be compared with the original fabrication data indications of gross dimensional changes. Table IX summarizes measurements of rod diameters from RML examinations of failed assemblies. Within the range of accuracy, it appears that little or no detectable diametral growth or change of length has taken place.

5.2.3 Microhardness Test

Microhardness tests were performed on a remotized Wilson Tukon Hardness Tester using a 136 degree diamond pyramid indenter with an applied load of 500 grams. The indentations were measured with a 40X objective lens and a filar eyepiece. Measurements are taken near the outside diameter, center, and inside diameter of the cladding. Figure 23 is a typical series of impressions. Table X summarizes the data taken during the course of examination. Comparative figures are tabulated for the Diamond Pyramid Hardness (DPH) on clad from the same lot of tubing prior to irradiation.

5.2.4 Burnup Analysis

Samples for burnup determinations are taken at RML by cutting sections of the fuel rod at the peak and average flux locations. Following radiochemical analysis the burnup is then calculated from the ratio of fission products such as Ce-144, Zr-95, or Cs-137 to uranium. On occasion as a final check a mass spectrographic analysis is run. In general, the mass spectrographic analysis has been the most reliable method.[23]

The burnup data for all rods analyzed is presented in Table XI. The burnup information obtained by physics calculations is included for comparison and is roughly within 10 percent.

5.2.5 Fission Gas Release

The procedure[24, 25] for determining the amount of fission gas release in a rod requires sampling in an RML cell followed by special analyses.

1. The plenum of the rod is sealed off in an evacuated system and then punctured.
2. Gamma count samples are aliquoted and analyzed for Kr-85.
3. Chromotographic samples are aliquoted for analysis of Kr, Xe, N_2 and O_2.

The quantities of Xe and Kr released noted in Table XII are negligibly small when considered as contributors to internal pressure in the fuel rod at power.

TABLE IX

POST-IRRADIATION MEASUREMENTS OF SELECTED RODS

Assembly Number	Rod No.	Clad Wall	Original Nominal OD ±0.002	Minimum OD Measured	Location (Inches from Top)	Maximum OD Measured	Location (Inches from Top)	Mean OD Measured
2D	A	0.012	0.398	0.396	4	0.404	2	0.400
2D	E	0.012	0.398	0.396	2, 4, 6, 10, 16, 18, 22, 26	0.402	38	0.398
2D	F	0.012	0.398	0.397	32	0.400	2, 12, 14, 18, 26, 34, 38	0.399
1G	B	0.014	0.358	0.360	All	0.362	1/4	0.361
1G	Q	0.014	0.358	0.356	40	0.361	2	0.359
1G	R	0.014	0.358	0.357	40	0.367	26 (defect)	0.361
1G	W	0.014	0.358	0.359	8, 10, 12	0.361	1/4 and 40	0.360
2G	B	0.014	0.358	0.356	20, 22, 26, 28	0.360	2	0.368
2G	G	0.014	0.358	0.358	4, 6, 8, 16, 18, 20, 34, 36	0.368	29 (defect)	0.362
3S	E	0.012	0.400	0.396	2, 37	0.461	12 (defect)	0.400

Range of accuracy is ±0.002 inches on diameter measurements.

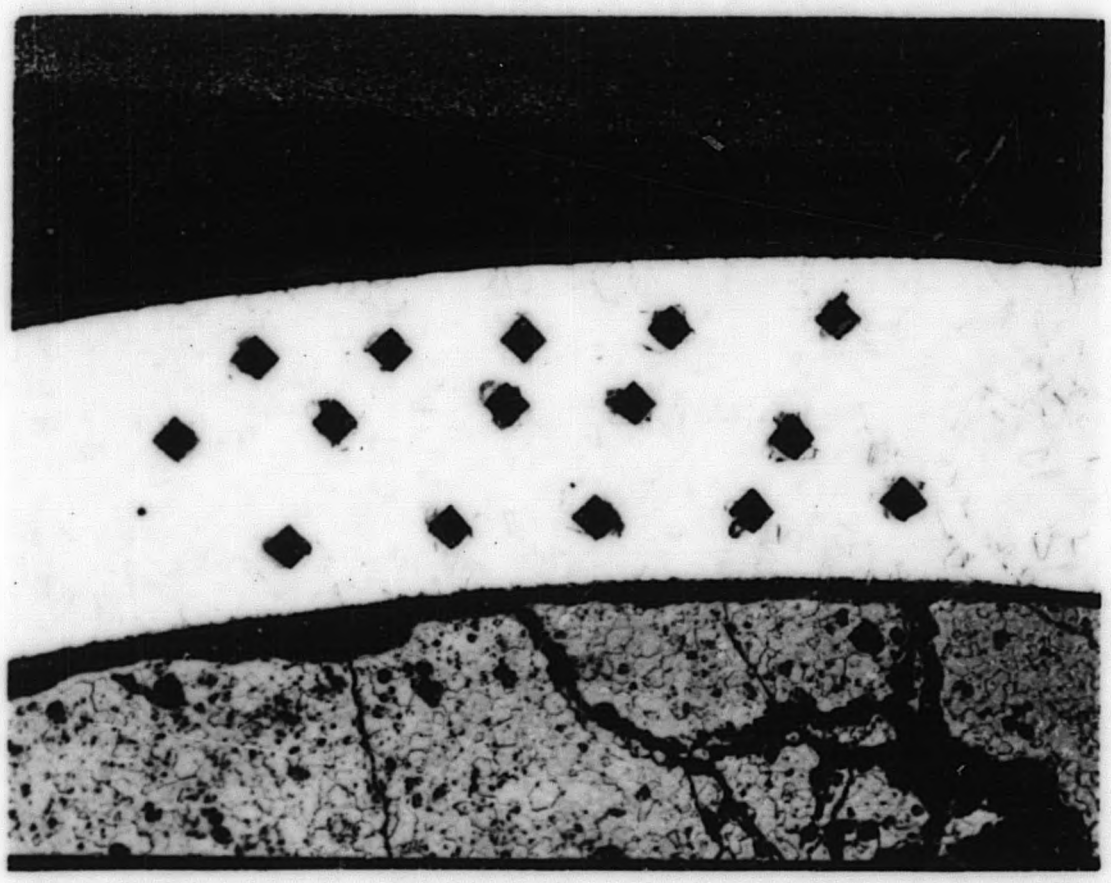

Etched 100X

Irradiated Cladding From HPD Fuel

Figure 23. Typical Microhardness Impressions

TABLE X

MICRO-HARDNESS DATA

Bundle Rod	Initial Tubing U. T. S.	Pre-Irradiation DPH(a)	Initial Clad Condition	Post-Irradiation DPH(b)	Exposure MWD/t (Calculated)	Exposure MWD/t (Measured)	ΔDPH	nvt > 1 mev × 10^{-20}	Location
1G-B	92,500	200	Ann	293	9600	--	93	10	Peak flux zone
1G-Q	110,000	240	Cw	305	9600	8600	65	10	Peak flux zone
1G-R	110,000	240	Cw	306	9600	6000	66	10	Peak flux zone
1G-W	92,500	200	Ann	284	9600	--	84	10	Peak flux zone
2G-G	110,000	240	Cw	328	9000	10500	88	10	Peak flux zone
2G-B	110,000	240	Cw	264	5600	4000	24	5.8	Low flux zone
2G-G	110,000	240	Cw	271	5600	--	31	5.8	Low flux zone
2D-A	112,000	242	Cw	284	4000	2800	42	6.72	Low flux zone
2D-E	112,000	242	Cw	342	6400	7000	100	10	Peak flux zone
2D-A	112,000	242	Cw	308	6400	--	66		Peak flux zone
3S-E	112,000	240	Cw	328	7200	8500	88	10	Peak flux zone
1E-E	112,000	240	Cw	294	10000	9800	54	10	Peak flux zone

(a) From References 10 and 18.

(b) Average of ~ 15 readings

TABLE XI

BURNUP DATA

ANALYTICAL vs CALCULATED

Bundle	Rod	Method of Measurement (a)	MWD/t Measured	MWD/t Calculated (b)
1G	Q	Mass Spectrometer	8700 peak	9600 peak
1G	R	Mass Spectrometer	6400 average	6000 average
2G	B	Ce-144/U	4300 average	5600 average
2G	G	Ce-144/U	11330 peak	9000 peak
2D	A	Ce-144/U	3100 average	4000 average
2D	E	Ce-144/U	7800 peak	6400 peak
3S	E	Ce-144/U	7400 peak	7200 peak
1E	E	Mass Spectrometer	9800 peak	10000 peak

(a) B. F. Rider, J. L. Russell, D. W. Harris, J. P. Peterson, "The Determination of Uranium Burnup in MWD/t", GEAP-3373, March 17, 1960.

(b) The portion roughly from 8 to 13 inches from the rod bottom is the peak flux region.

TABLE XII

FISSION GAS RELEASE

Bundle	Average Burnup	Maximum UO_2 Temperature	Average Centerline Temperature	Rod	Total Gas Volume Released (cc)	Aliquot Sample Volume (cc) (a)	Atoms Kr-85 Released Per Rod	Constituents (a) Analyzed $\times 10^{-3}$ cc					Percent Fission Gas Released of Fission Gas Formed
								O_2	N_2	Kr	Xe	Xe/Kr	
2G	5600 MWD/t	3050°F	1900°F	B	3.45	0.314	3.71×10^{16}	1.3	1.9	2.0	12.9	6.5	0.209%
2G				B		0.285		9.0		1.9	12.5	6.6	0.224%
2D	4000 MWD/t	2900°F	1800°F	F	5.01	0.350	3.29×10^{16}	1.4	3.1	1.2	8.5	7.1	0.152%
2D				F		0.325		1.0	3.1	1.1	8.2	7.4	0.158%

(a) Constituents analyzed $\times 10^{-3}$ + He (added during fabrication) = Sample Volume

The curve shown in Figure 24 was first published in June, 1963, as part of the Transactions of the American Nuclear Society, Volume 6, Number 1.[28]

Although the average burnup achieved for the HPD fuel is in the range presented on the curve, the relatively low average centerline temperature probably accounts for the low fission gas release. The average centerline temperatures given is only for those conditions present at maximum reactor power (between 30 and 40 MWT). In the case of HPD fuel the maximum power conditions were only present approximately 70 percent of the time.

5.2.6 Metallography of 1G

Selected fuel rods from six assemblies have been examined by metallographic methods as noted in Table VII and two more rods are in progress. The number of rods checked metallographically is 13. The metallography performed on Assembly 1G is presented in detail since it is considered representative of what has been observed in other HPD rod failures.

The visually observed cracks in HPD 1G are typical of all HPD failures to date, with the exception of 4E and 6S. The cracks in annealed rod C in the 4E failure were circumferential, while the others were predominantly longitudina' Assembly 6S displayed a combination of circumferential and longitudinal cracks in two rods. Another distinction may be noted regarding macroscopic appearance: 1G shows relatively severe cracking and in general represents the swaged pellet and powder fuel in this respect. The free-standing fuel rods with few exceptions have shown much smaller cracks, sometimes very difficult to locate. Metallographic specimens are selected based on the condition of the failure and generally are transverse cross sections which reveal the longitudinal cracks. In a few cases a longitudinal specimen was cut from the rod in question because of the type of failure present. This was done in assembly 3S, Rod E, and assembly 4E, Rod C.

The metallographic specimens were prepared in the following manner:

1. Vacuum potted in Bakelite mounts with Hysol epoxy resin.
2. Ground on successive silicon carbide papers through grit.
3. Polished: (a) 3μ diamond paste on nylon cloth,
   (b) 1μ diamond paste on nylon cloth,
   (c) $\frac{1}{2}\mu$ diamond paste on "MOL" cloth.
4. Cladding etched for carbides using ASTM Special Technical Publication 110 procedure.
5. Cladding etched electrolytically with 10 percent oxalic acid to reveal general microstructure.
6. Fuel etched with 10 percent HNO_3, 20 percent H_2O_2 (30 percent) and 70 percent H_2O.

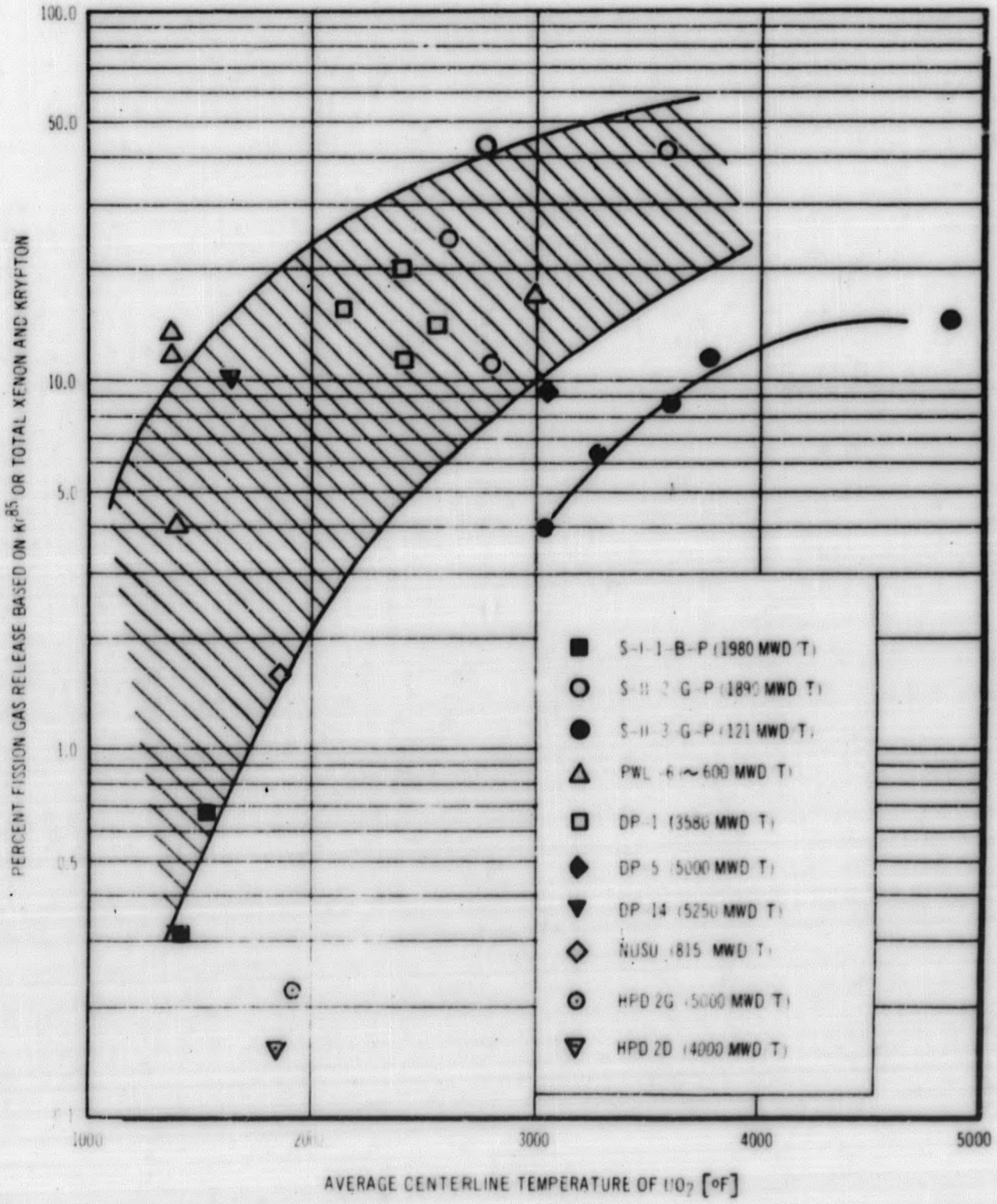

Figure 24. Fission Gas Release (As a Function of the Calculated Average Centerline Temperature of UO_2 During Maximum Power Operation)

HPD 1G Failure Analysis

Four rods were analyzed in detail. Rods B and W were sound rods and R and Q were failed rods. Rod R, the (visually detected) failed rod, was examined to determine the nature of the failure. Rod Q (nothing detected visually) had large ultrasonic signals and was examined to verify these signals. In addition to the "standard" examinations, tensile and burst tests were performed on all four rods.

Rod B, Sound Rod

A gamma scan, Figure 26, was run on the rod to determine the exact location of the peak flux zone. The rod was then sectioned at this zone for a metallographic sample.

The cross section of the clad and fuel is shown in Figure 25 with typical photomicrographs indicated.

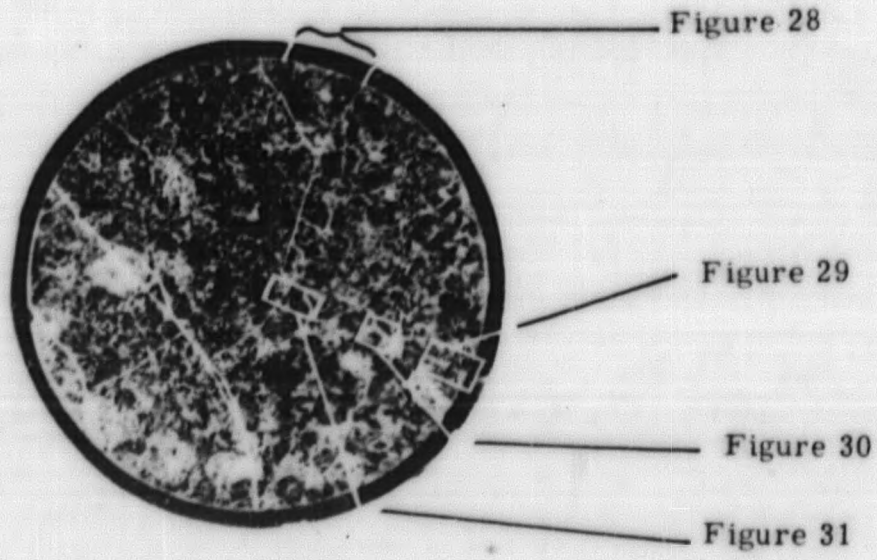

Figure 25. Metallographic Specimen from HPD 1G, Rod B

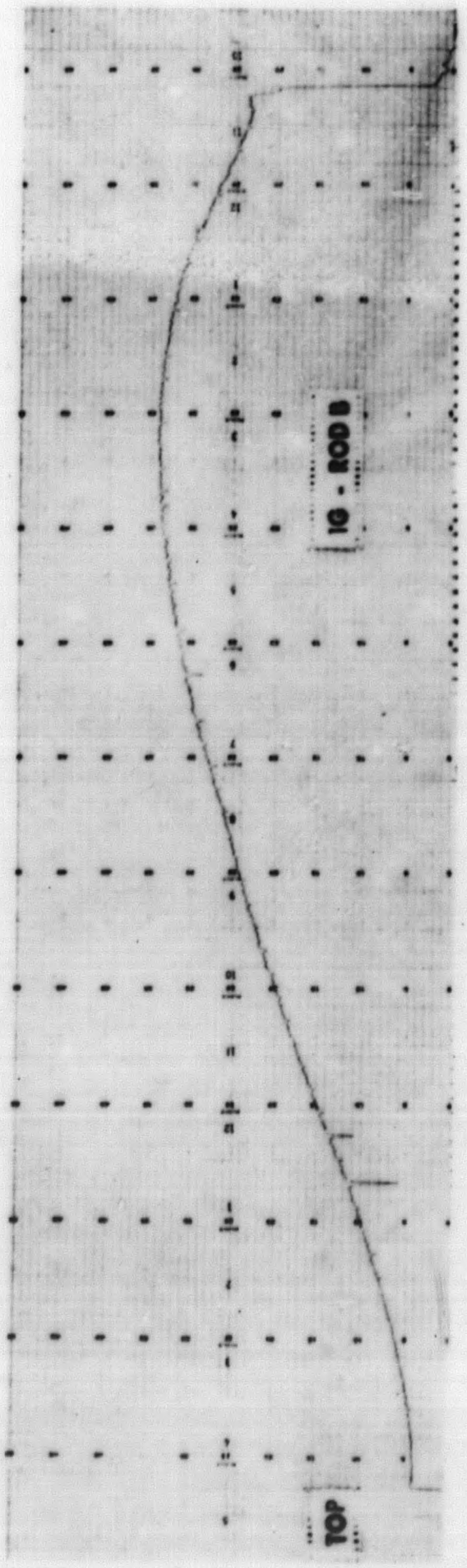

Figure 26. Gamma Scan of HPD 1G, Rod B

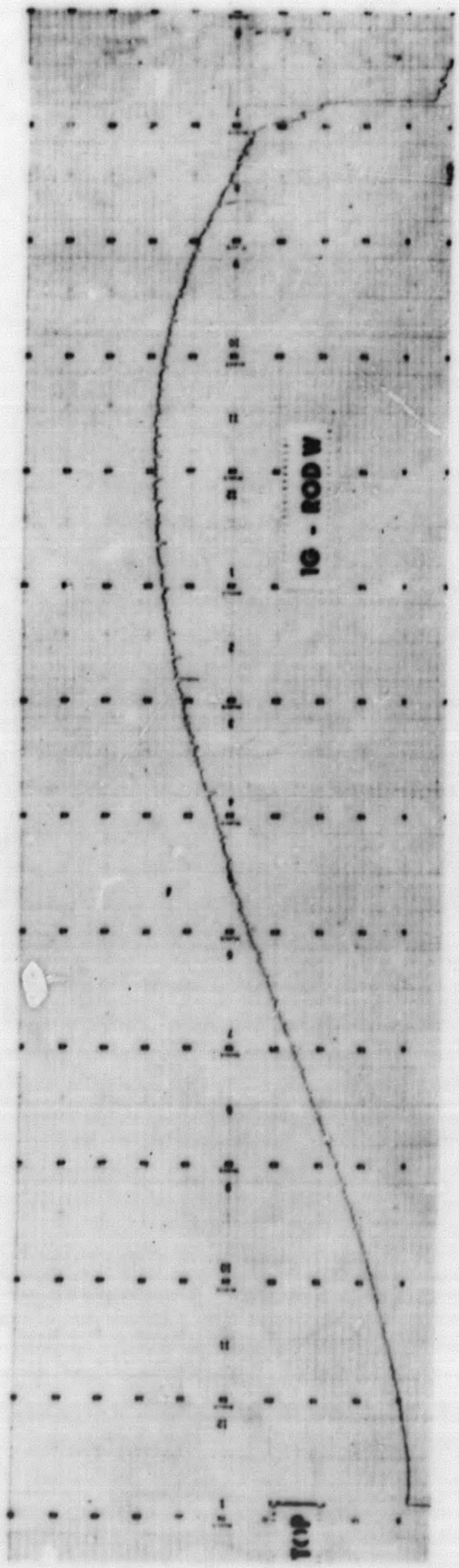

Figure 27. Gamma Scan of HPD 1G, Rod W

The cladding, prior to irradiation, was in the commercially annealed condition. The absence of slip-lines in the microstructure shown in Figure 28 is typical of annealed material. The narrow zone observable at the inner surface of the clad is believed due to fission fragments and is typical of stainless steel cladding studied in the HPD program. The metallographic investigations with the optical microscope thus far have been unable to detect any significant sensitization of the clad structure. The small cold worked dent at the surface of the section shown in Figure 28 is of unknown origin.

The UO_2 fuel structure is equiaxed and showed essentially no variation in grain size from the core to the interface with the clad. This is observable in Figures 29, 30, and 31. Extensive porosity occurred in the UO_2 matrix primarily at the outer edge of the pellet. At the mid-radius and the center of the fuel, porosity was visible in the grain boundaries and matrix.

The appearance of the cladding and fuel in this rod is typical of sound pellet type fuel rods after irradiation to approximately 8,000 MWD/t.

Rod W

Rod W exhibited the same appearance metallographically as Rod B. A gamma scan of Rod W is shown in Figure 27.

Rod R and Q

These rods revealed cracks in the peak flux region. Prior to irradiation the cladding was in a cold-worked condition in both rods.

Rod Q showed two deep cracks (Figure 33) in the cladding with a penetration of ~90 per cent of the cladding thickness and were first detected by ultrasonics (Table VIII). A possible growth pattern of the cracking process is illustrated by Figures 32a, 32b, 32c from a pit in the surface to cracks of different degrees of penetration. These photomicrographs are of different locations on a single cross section. The cracking pattern in both specimens was definitely intergranular.

Figure 34 is a macrophoto of the cross section of cladding and fuel examined from Rod R (the main cracked region) and shows the location of multiple cracks and partial cracks. Figure 35 is a photomicrograph of one of these large cracks.

The many cracks in the section of cladding illustrate the severity of failure. See Figure 12 for the macroscopic view of the failed rod.

Corrosion Product in Cracks

Inspection of Figure 36 reveals a sizeable "nugget" of what is assumed to be an oxide corrosion product. Figure 37 shows a similar appearing oxide along the crack interface. Analysis will be attempted of the nugget material. These observations of oxide have not always been

Outer Surface of Clad

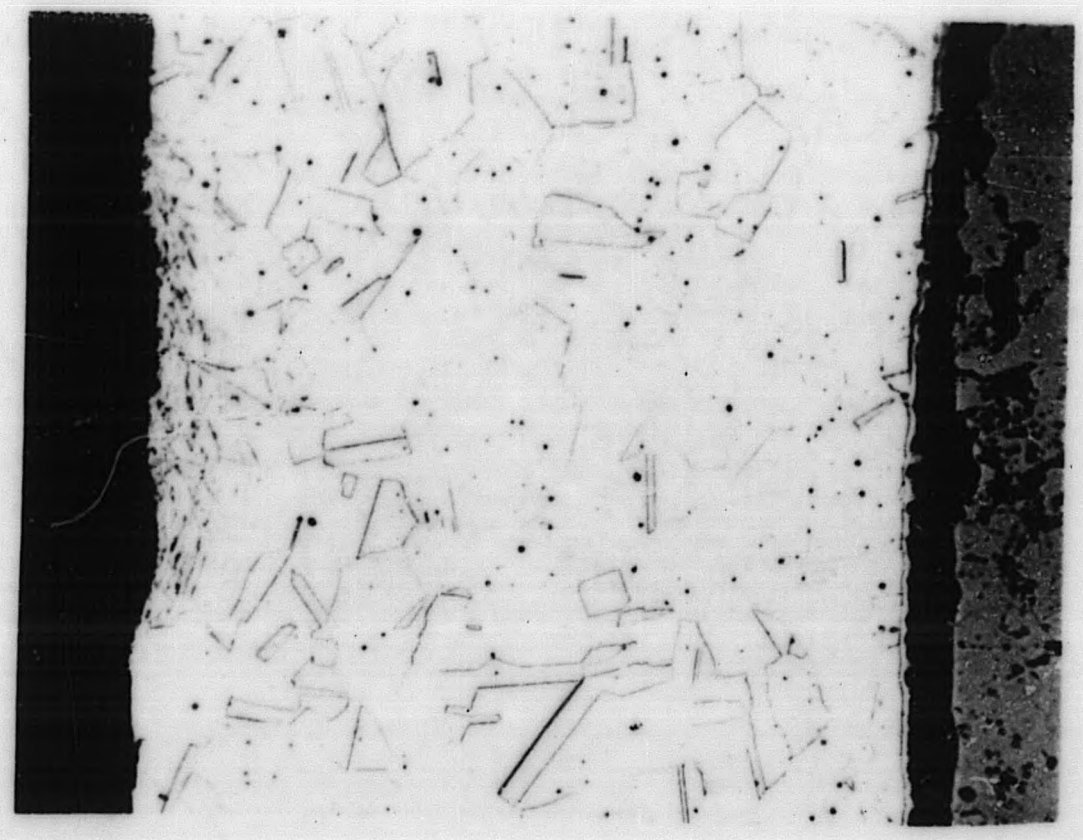

Inner Surface of Clad

8623-05 Etched 250×

Initially Annealed Material

Figure 28. Cross Section of Clad from HPD 1G, Rod B

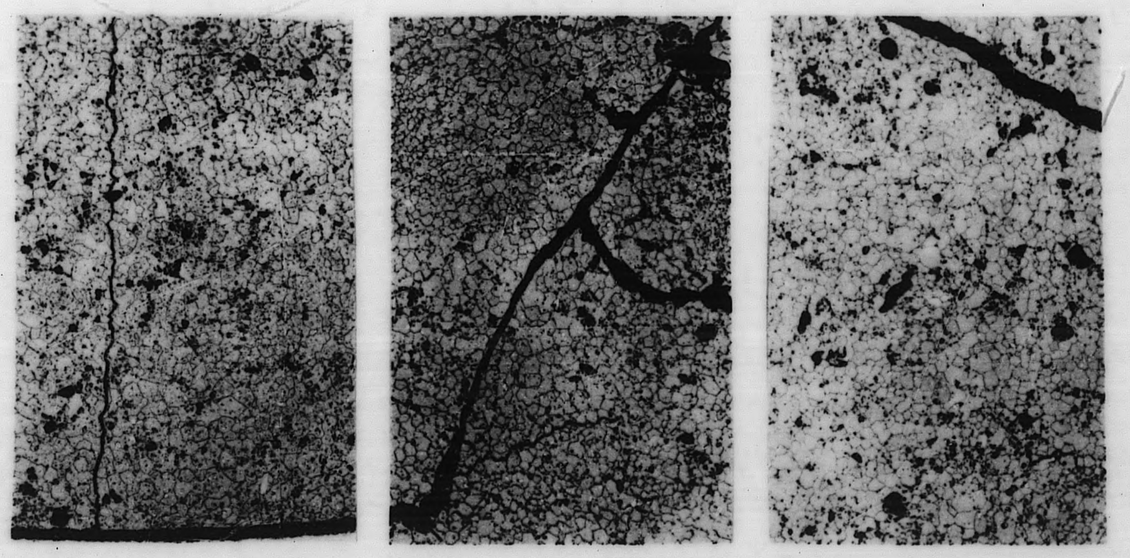

100×
Etched

8623-17

100×
Etched

8623-16

100×

8623-15

Figure 29. Typical UO_2 Fuel - Clad Interface HPD 1G, Rod B

Figure 30. Typical UO_2 Fuel at Mid-Radius HPD 1G, Rod B

Figure 31. Typical UO_2 Fuel at Center HPD 1G, Rod B

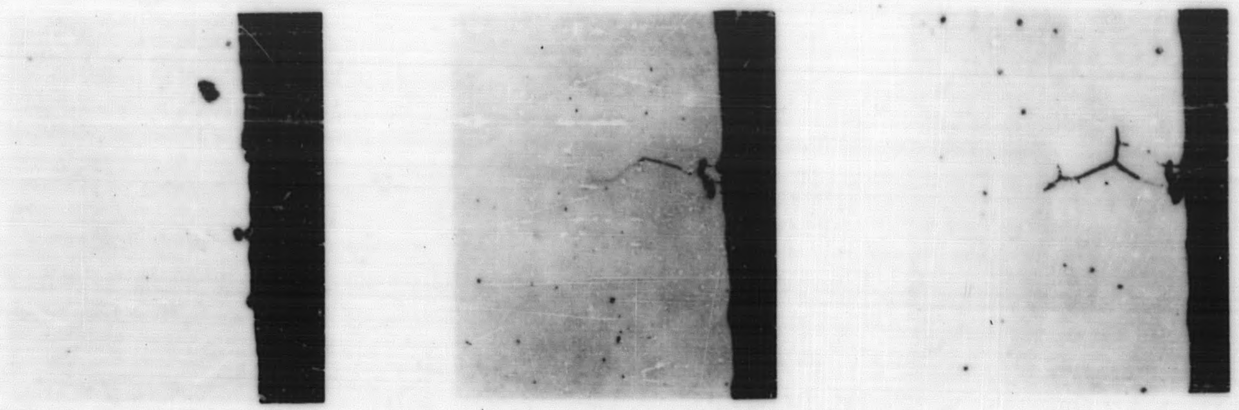

32a			32b			32c		
8624-11	Polished	500×	8624-06	Polished	500×	8624-12	Polished	500×

Figure 32. Assumed Mode of Crack Propagation from Outside Surface Toward Inside Surface of Clad. Photomicrographs Are of Different Sections of Same Polished Specimen. Assembly 1G. Rod Q.

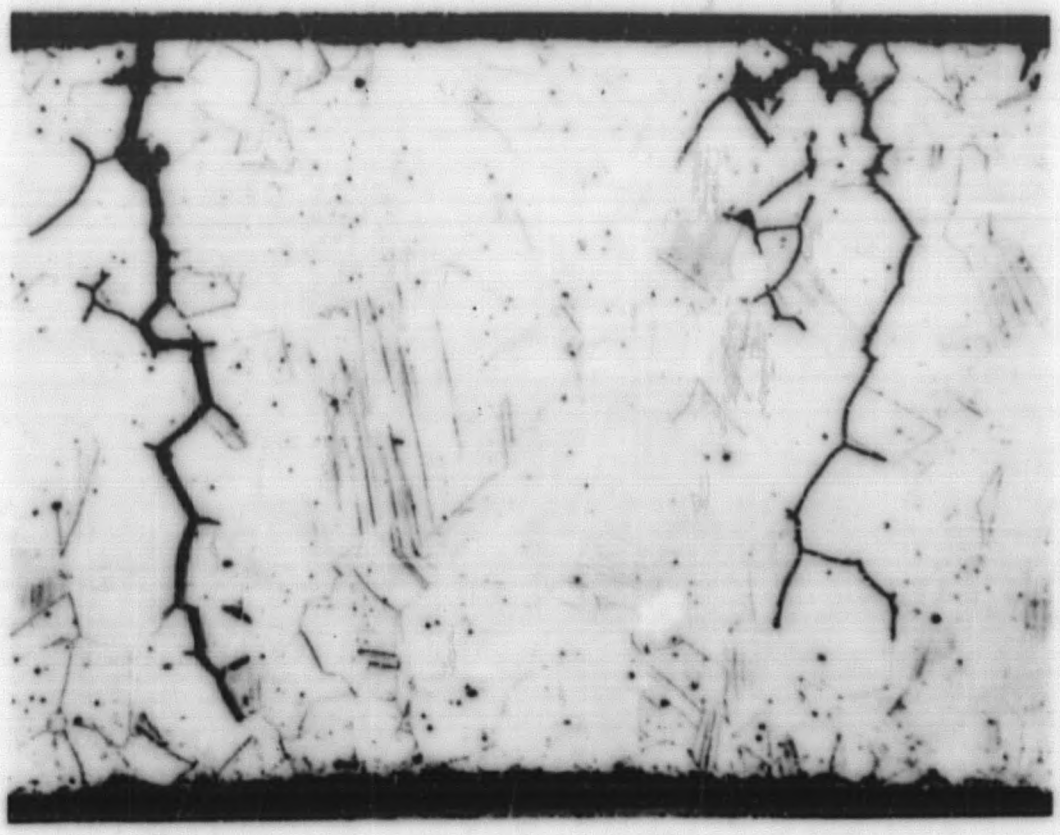

8624-10 Etched 250×

Cold-worked structure and intergranular attack.

Figure 33. Cracks in Clad of Rod Q, HPD 1G

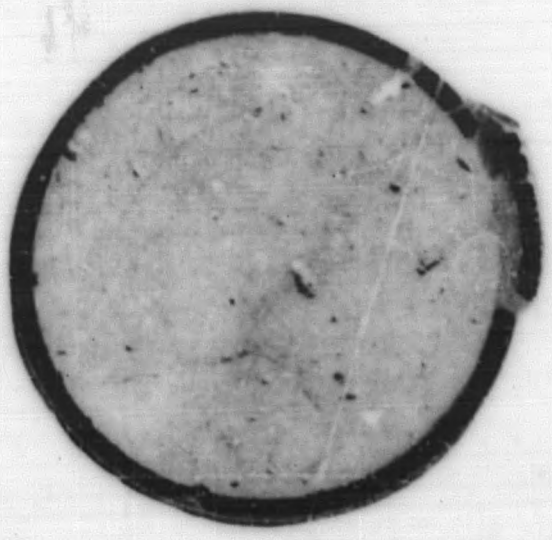

8625-01
1G - Rod R
Clad Fuel Specimen
As Polished

Figure 34. Cross Section of Cladding at Failure Location Rod R of HPD 1G

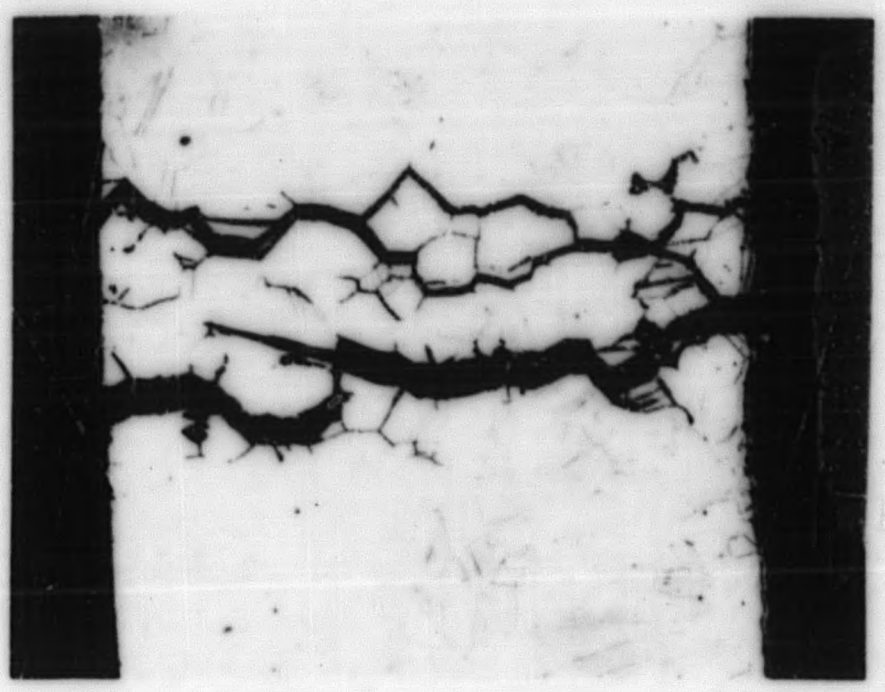

Figure 35. Intergranular Cracks in Initially Cold Worked Cladding From Rod R, Assembly 1G. (Peak Flux Location. 250×)

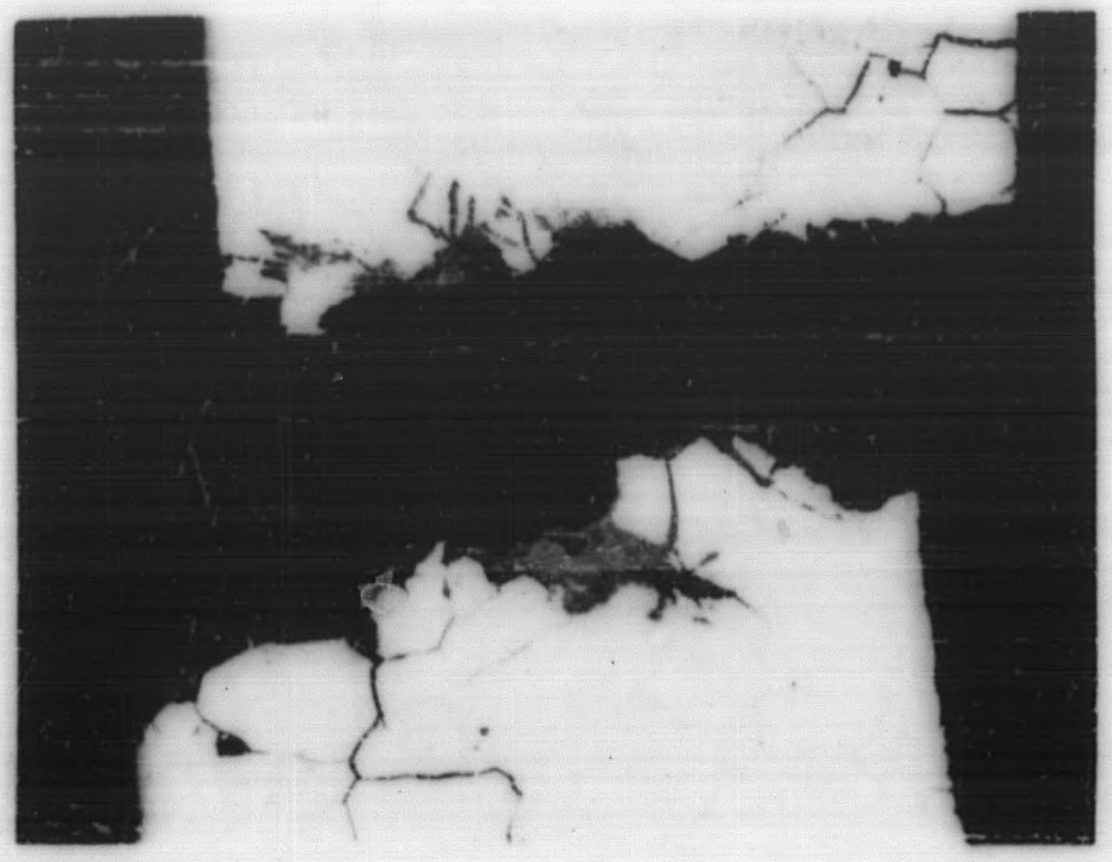

250×

Figure 36. Section of Rod R, HPD 1G, Showing "Nugget" of Corrosion Product Near Mid-Thickness of Cladding

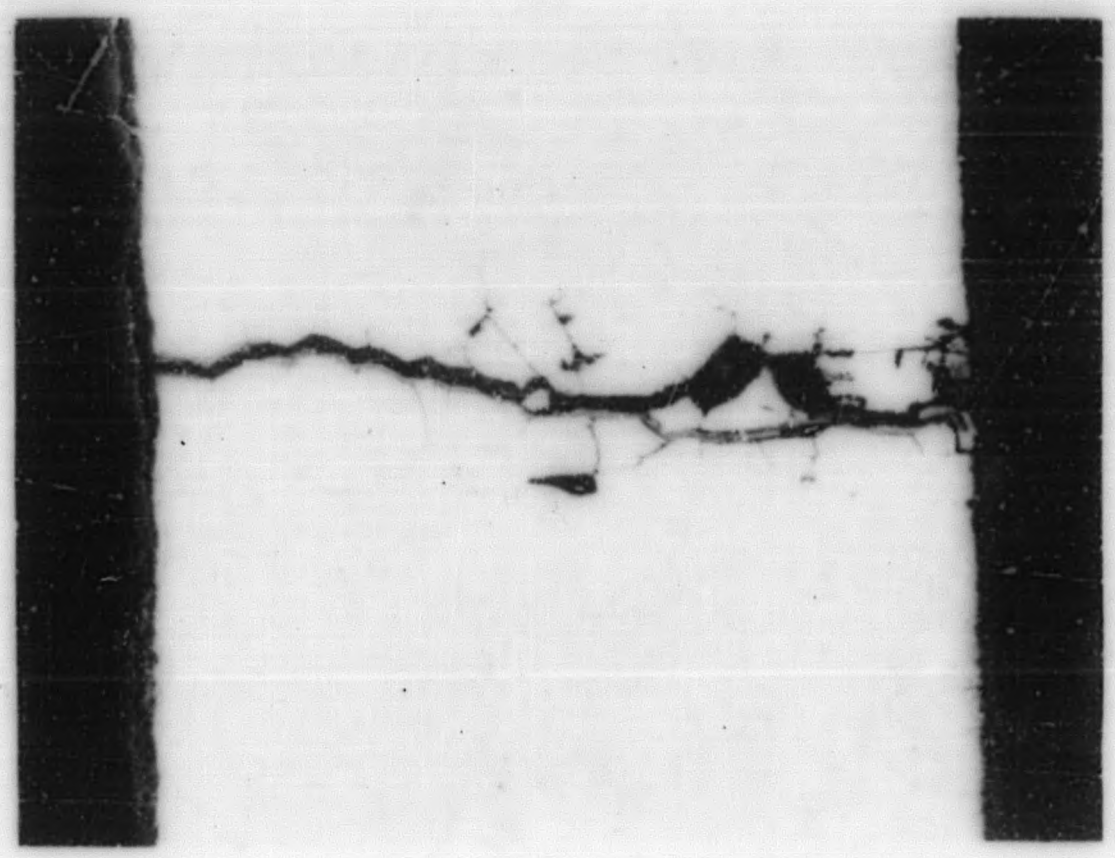

250×

Figure 37. Section of Rod R, HPD 1G, Reveals Uniform Layer of Corrosion Product in Fracture

maoe in the case of most other metallographic specimens of cracked cladding. It is not known how typical such relatively gross quantities of corrosion product are in the many fuel failures. However, inasmuch as the time of formation of the crack relative to removal of the fuel rod from the reactor is not known, it is possible for buildup of corrosion products to occur during continued irradiation of the cracked fuel rod. It is also possible that the corrosion product is formed during storage prior to examination.

5.2.7 Tensile Testing 1G

Samples from the cladding from Rods B, W, R and Q were prepared for elevated temperature tensile testing. Two specimens each were cut from the peak and average flux regions of each rod. The UO_2 was removed mechanically taking care that the cladding curvature remained undisturbed. Tests were conducted with a Tinius Olsen 60,000 pound electromatic testing machine at a temperature of 625 F ±15 F. Cross head movement was transmitted from an Olsen D2 deflectometer, and was kept below 0.020 inch per minute.

The data in Table XIII indicate that at a fast flux exposure of 10^{21} nvt, the 625 F yield strength of initially annealed clad is about 100,000 psi and cold work clad is about 118,000 psi. The data also show that at 10^{21} nvt the yield strength of the annealed material is approximately double that in the unirradiated condition. Figure 38 shows the typical tensile specimens after testing at 625 F. Photos of the tensile test equipment and fixtures developed for the HPD program are shown in Figures 39, 40 and 41.

Effects of irradiation on Clad Yield Strength

The increase in yield strength of austenitic stainless steel, which normally occurs under irradiation, is an important consideration. A search has been made of the literature for work in the area of high temperature irradiation and high temperature testing of stainless steel. The scarcity of data available is apparent when the curve in Figure 42 is examined. Included are data from the AEC Fuel Cycle program[29] and HAPO[30] as well as that from the HPD program.

In general work done in the area of irradiation hardening, mainly at low temperature irradiation, tends to indicate that the magnitude of the increase of yield strength decreases with increasing levels of cold work. Figure 42 corroborates this by the appearance of two separate curves, one for cold work material of the level used in the HPD series, and one for the commercially annealed material. The limited data available do not reveal what happens as exposure of the clad goes beyond 10^{21} nvt >1 mev. It is possible that a level of equilibrium may develop whereupon the effects of recovery at operating temperature and continued irradiation hardening may tend to compensate. In the event that this occurs the two levels of cold work presented on this chart might either approach each other at some higher exposure level or remain separated by approximately the same difference in yield strength that occurs at lower exposures.

TABLE XIII

ELEVATED TEMPERATURE (625°F) TENSILE PROPERTIES OF IRRADIATED 304 STAINLESS FUEL CLAD FROM ASSEMBLY 1G

Sample Identity (a)	0.2 Offset Yield Strength of Initial Clad Condition (b)	Clad Exposure (nvt > 1 Mev × 10^{-21})	0.2 Offset Yield Strength (psi)	Ultimate Tensile Strength (psi)	Elongation (% in 0.8 inches)
B-3	45,000 Ann	1.0	90,900	97,400	8.0
B-3	45,000 Ann	1.0	104,000	104,000	6.1
B-1C	45,000 Ann	0.6	75,000	84,200	6.6
B-1C	45,000 Ann	0.6	71,200	85,500	6.8
W-3	45,000 Ann	1.0	99,000	99,400	4.4
W-3	45,000 Ann	1.0	107,200	108,300	2.8
W-1	45,000 Ann	0.6	76,300	81,700	5.5
W-1	45,000 Ann	0.6	76,200	87,500	7.8
Q-5	94,000 Cw	1.0	117,000	118,000	1.4
Q-5	94,000 Cw	1.0	120,000	121,000	2.3
Q-2	94,000 Cw	0.6	91,100	98,600	4.0
Q-2	94,000 Cw	0.6	111,900	118,700	3.9
R-5(c)	94,000 Cw	1.0	72,500	72,500	2.5
R-5(c)	94,000 Cw	1.0	39,700	40,900	3.8
R-1	94,000 Cw	0.6	112,408	115,000	4.0
R-1	94,000 Cw	0.6	104,300	108,000	3.8

(a) Letter indicates fuel rod

(b) Ann - annealed; Cw - cold work, properties at room temperature

(c) Samples contained longitudinal cracks

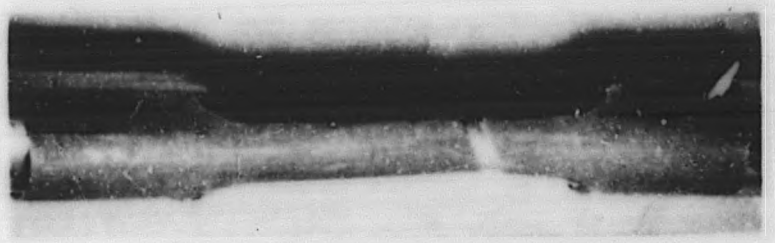

Irradiated ($\times 10^{21}$ nvt)
Initially Annealed Clad (Rod B)

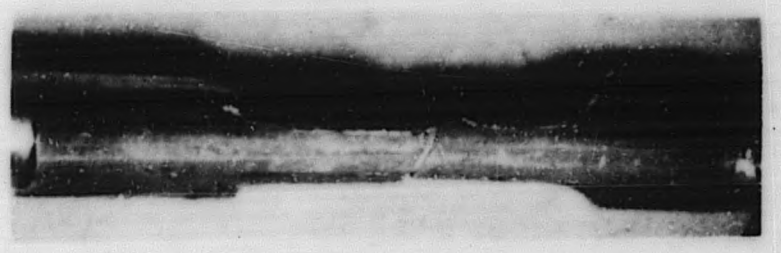

Irradiated ($\times 10^{21}$ nvt)
Initially Cold Work Clad (Rod Q)

Irradiated ($\times 10^{21}$ nvt)
Initially Cold Work Clad (Rod R)
Sample Contained Longitudinal Cracks

Figure 38. Photographs of Tensile Specimens After Testing at 625 F

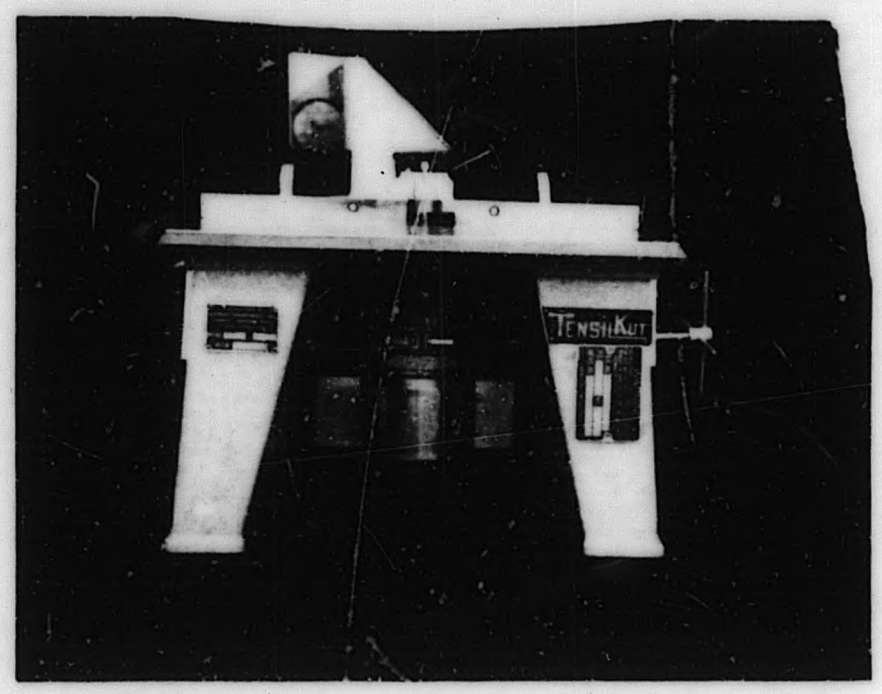

Figure 39. Micro-Specimen Cutter

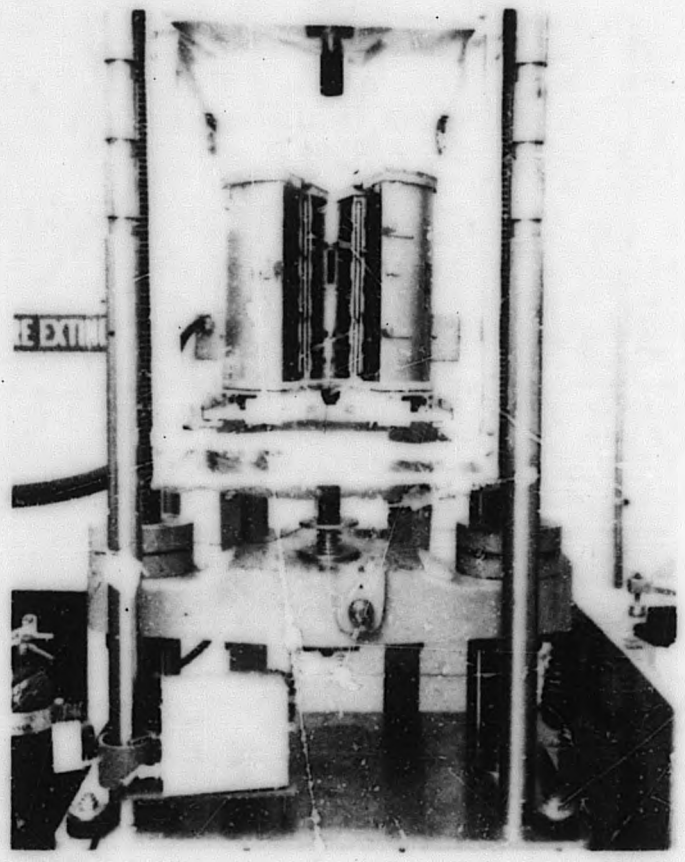

Figure 40. Test Setup in Tensile Testing Machine

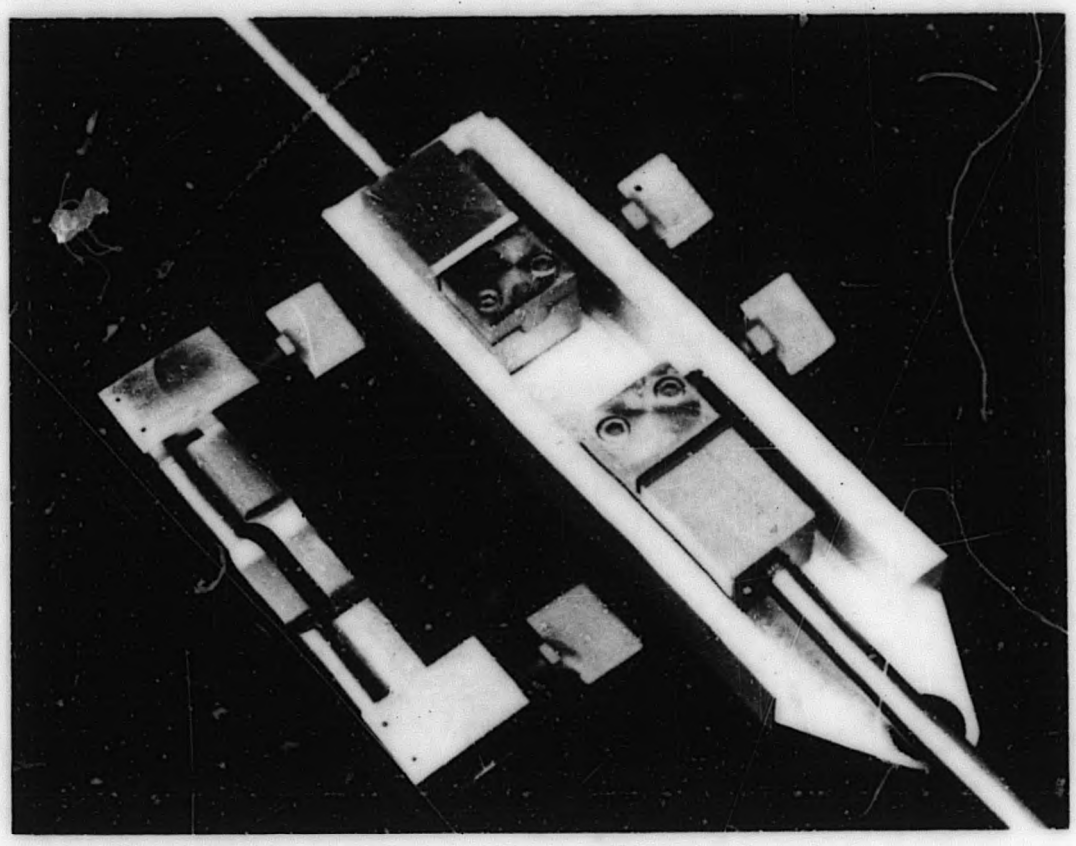

Figure 41. Tensile Grips and Template

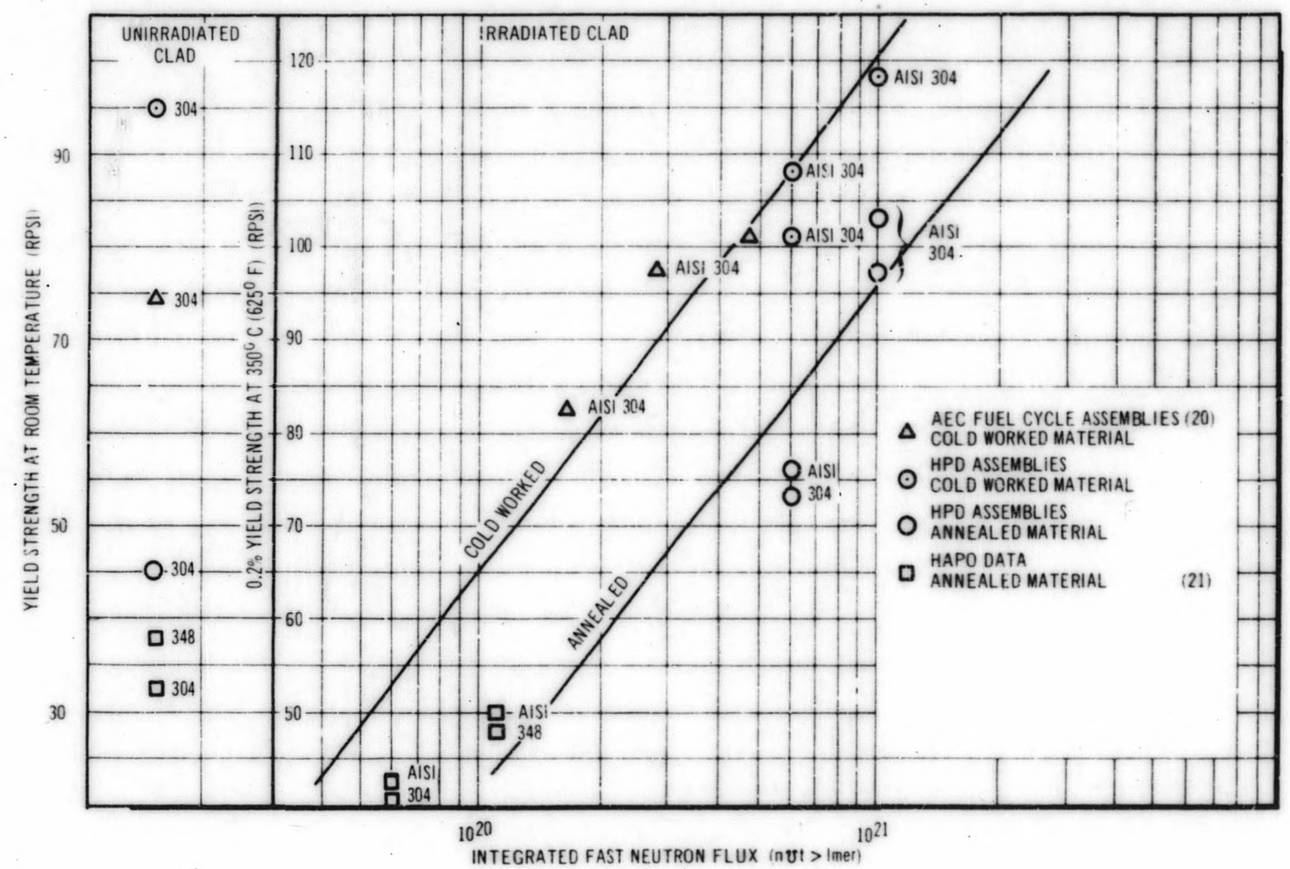

Figure 42. Irradiated Clad 350°C (625°F) Yield Strength vs Integrated Fast Neutron Flux >1 Mev

5.2.8 Burst Testing 1G

Elevated temperature burst testing was run on samples taken from two annealed rods (B and W) and two cold worked rods (Q and R) from HPD 1G assembly. Fuel rod segments, 5.25 inches in length, were removed from peak and average flux regions of the rods. Testing was done on two segments from each rod.

A hydrostatic pressure testing device using silicone rubber O-rings and Parbak backup rings for sealing was designed and fabricated for this work. (See Figure 43.) An air-operated Sprague hydraulic pump provided pressures in conjunction with an 0-10 millivolt recorder and pressure readings were obtained after the completion of the tests. The accuracy of pressure measurements was within ±500 psi. A special fire resistant hydraulic fluid of triaryl phosphates was used for the tests. An electric circulating air type oven was used to provide the source of heat. The oven was adapted so that the burst fixture could be rolled in and out for each test. Temperature measurements were obtained through (2) clip-on chromel alumel thermocouple leads which were attached to the specimens prior to each test. Test temperature measurements were all within the range of minus 5F, plus 20F.

Figures 44 through 49 reveal that appreciable ductility is present in the irradiated cladding (average exposure ~6,000 MWD/t and maximum exposure ~9,600 MWD/t).

It is evident from Table XIV that the percent change in diameter corroborates the qualitative visual observation made above that the material has retained good ductility. The hoop stress (Table XV) at bursting agrees reasonably with the tensile breaking strength reported in Table XIII. Note that the tensile tests were performed at 625 F, somewhat higher than the burst tests which were conducted at 550 F and 600 F.

5.2.9 Crud Analysis

All rods in the VBWR have a reddish oxide film on their surfaces after irradiation. Table XVI presents the results of the chemical analysis on several rods sampled after being stored in the VBWR pool. Additional analyses of the crud film taken from rods in the VBWR will be made to eliminate the possibility that any error is introduced by exposure to different purity water.

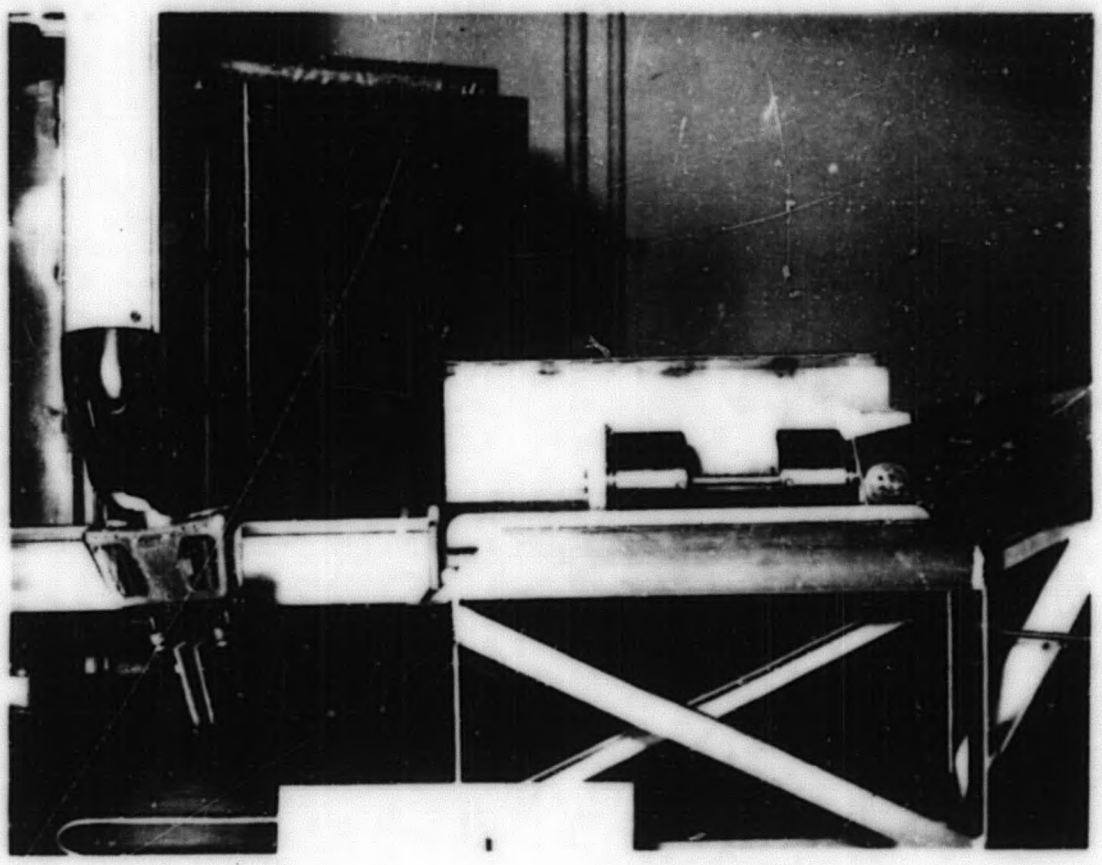

Figure 43. Hydrostatic Pressure Fixture With Burst Sample in Place

Figure 44. Burst Test Sample, Annealed HPD, Rod B Avg., 1 G

Figure 45. Burst Test Sample, Annealed HPD, Rod B Peak, 1 G

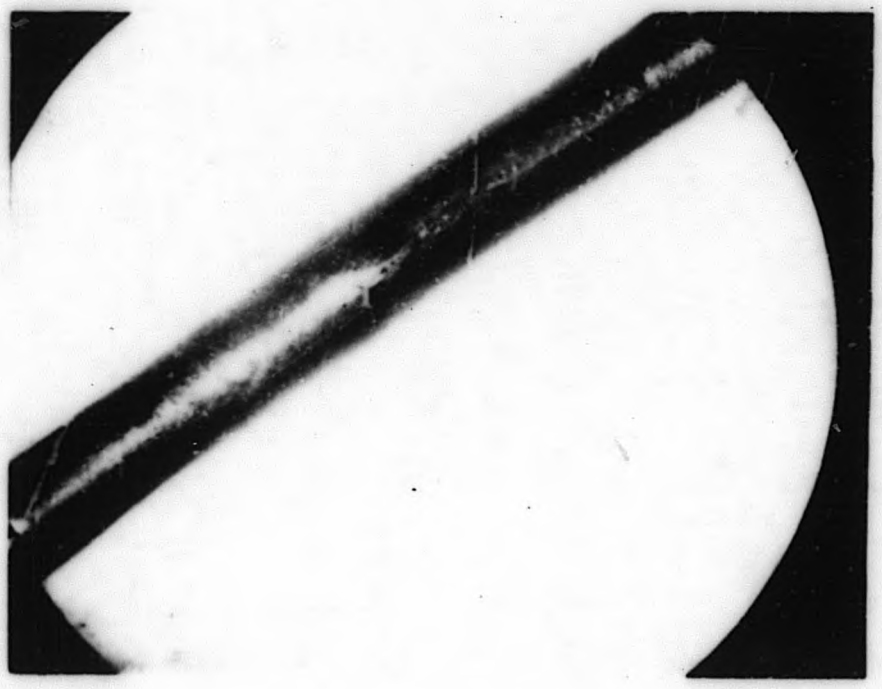

Figure 46. Burst Test Sample, Cold Worked HPD, Rod Q Avg., 1G

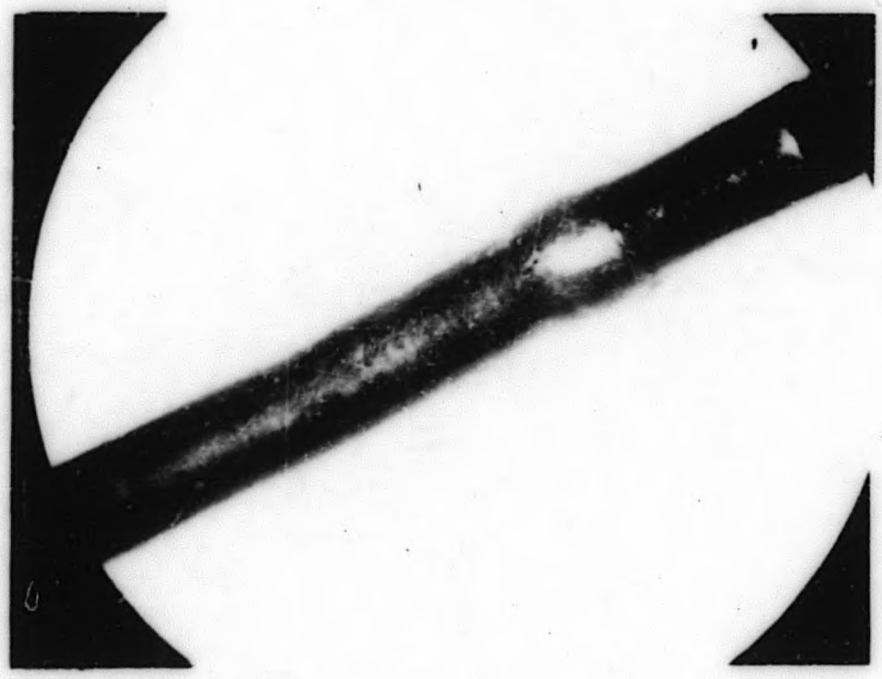

Figure 47. Burst Test Sample, Cold Worked HPD, Rod R Avg., 1 G

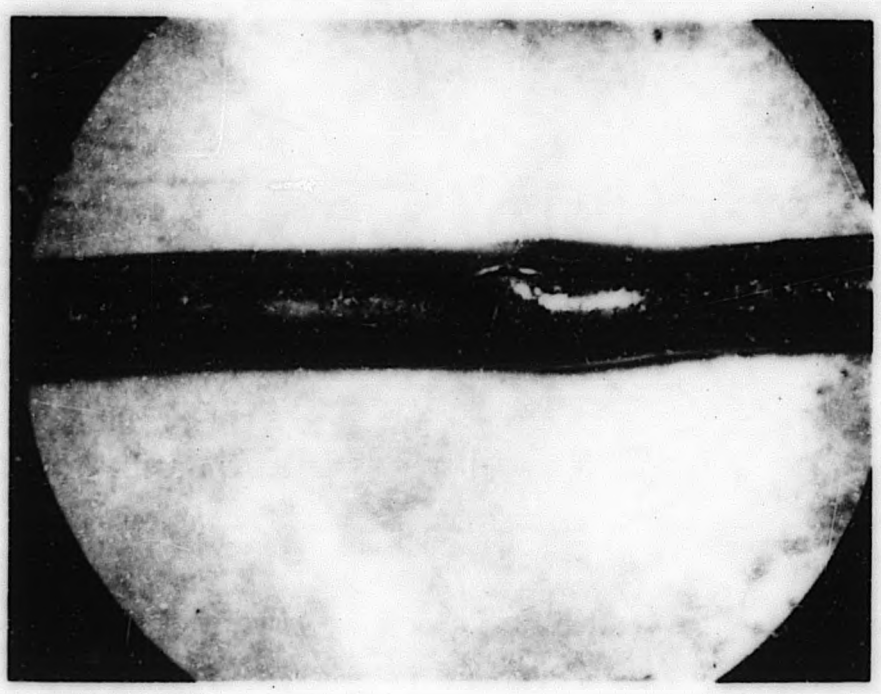

Figure 48. Burst Test Sample, Annealed HPD, Rod W Avg., 1 G

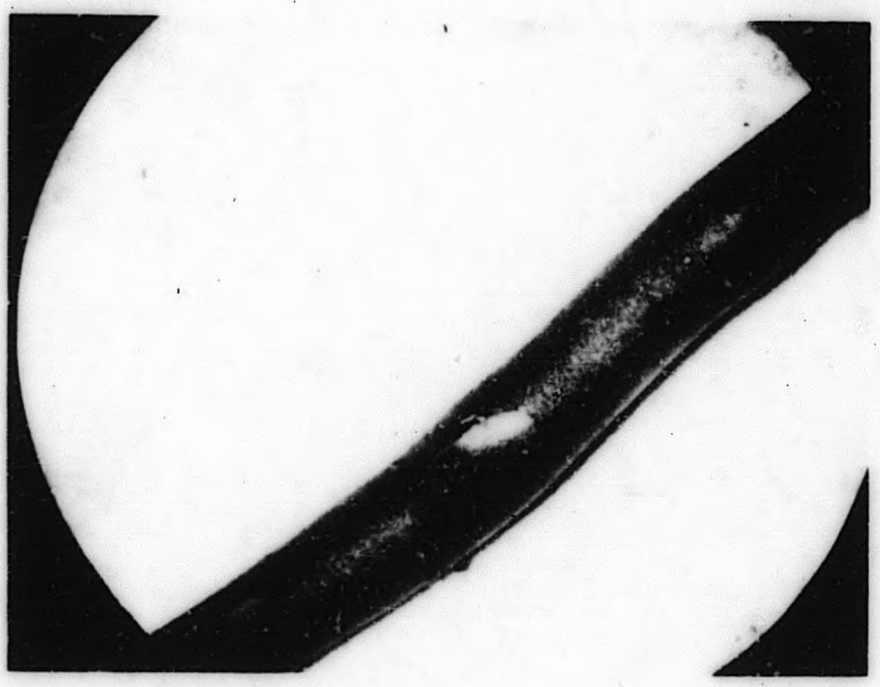

Figure 49. Burst Test Sample, Annealed HPD, Rod W Peak, 1 G

TABLE XIV

DUCTILITY OF BURST TEST SAMPLES

Sample[a]	O. D_0[b]	O. D_1[c]	O. D_2[d]	$\Delta D\%$[e]
1G-B-P	0.359	0.419	0.413	15.0
1G-B-A	0.358	0.419	0.414	15.6
1G-W-P	0.359	0.423	0.412	14.8
1G-W-A	0.359	0.449	0.434	20.9
1G-R-P	0.360	--	--	--
1G-R-A	0.361	0.440	0.439	21.6
1G-Q-P	0.360	--	--	--
1G-Q-A	0.361	0.408	0.398	10.2

(a) Bundle, rod, peak or average flux, B and W were annealed; R and Q cold worked.

(b) Original diameter

(c) Diameter across rupture region

(d) Diameter at 90° from rupture region

(e) $\frac{D_2 - D_0}{D_0} \times 100$

TABLE XV

STRENGTH OF BURST TEST SAMPLES

Sample[a] Identity	Burst Temperature (°F)	Burst Pressure (psi)	Circumferential Hoop Stress (psi)	For Comparison-- Ultimate Tensile Strength psi at 625 F from Table XIII
1G-B-P	550	8700	111,000	101,000
1G-B-A	600	7500	95,900	84,800
1G-W-P	500	8400	108,000	103,800
1G-W-A	600	7100	91,000	84,600
1G-R-P	600	(b)	---	---
1G-R-A	600	8400	108,000	112,500
1G-Q-P	550	(b)	---	119,500
1G-Q-A	600	(c)	---	108,600

(a) Bundle, rod, peak or average flux, B and W were annealed; R and Q were cold worked

(b) Pressurized at 19,000-20,000 psi, but fluid did not penetrate the fuel compact

(c) The sample burst at an unknown pressure at ~20,000 psi pressure drop across the fuel compact was being recorded

TABLE XVI

CRUD ANALYSIS

Assembly and Rod No.	mg Fe/mg Sample		$\mu g\ Cl^-$/mg Sample	
	Top	Bottom	Top	Bottom
2G B	4030	3850	4	14
2G G	510	410	8	6
1E		494		0.32*
2D A	210		16	
2D E	30		20	

*320 ppm.

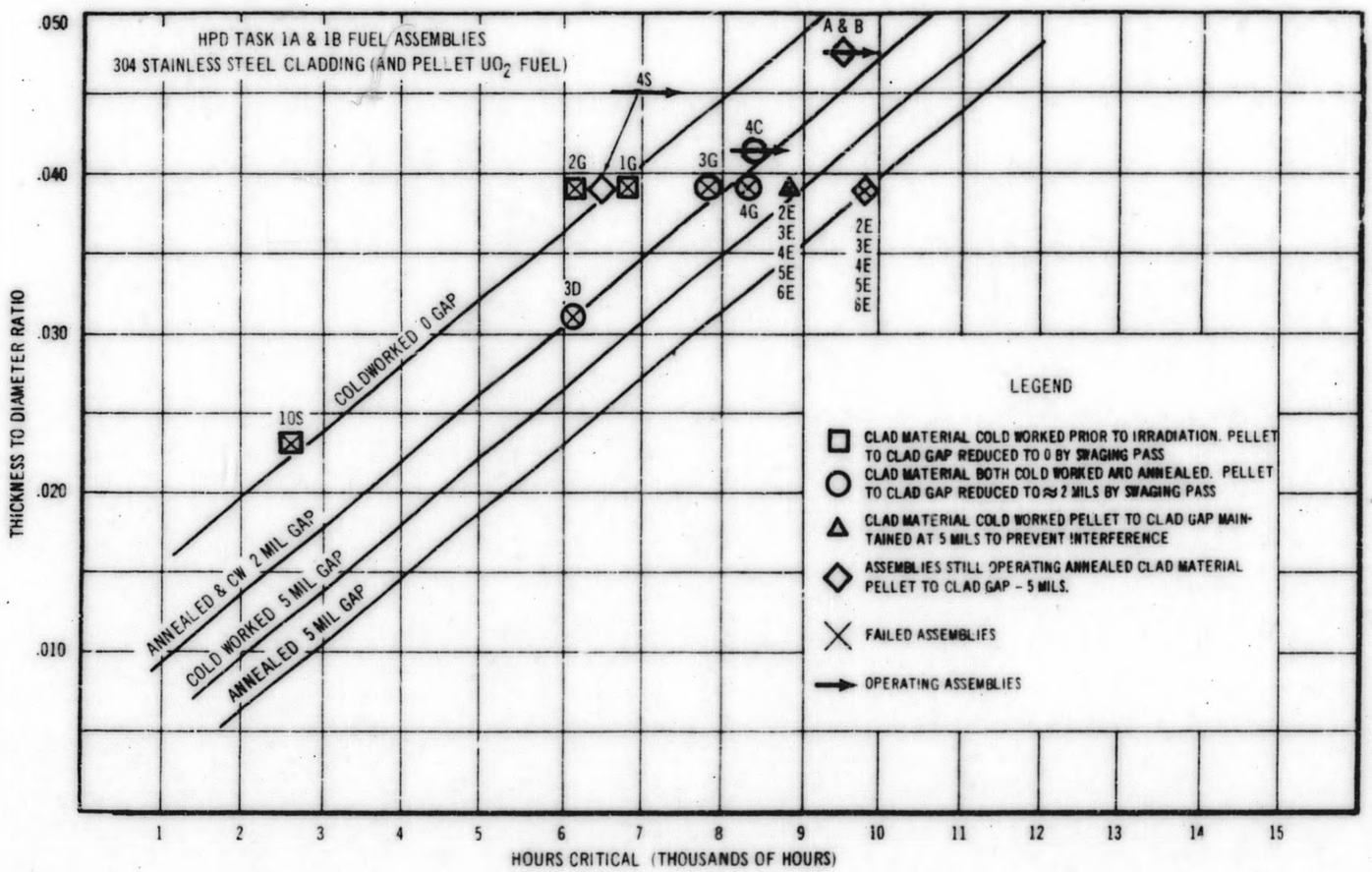

Figure 50. Fuel Lifetime (hours critical) vs t/D for Operating Fuel and Failed Fuel

APPENDIX A

Additional Pictures
Annealed Rod C, Assembly 4E

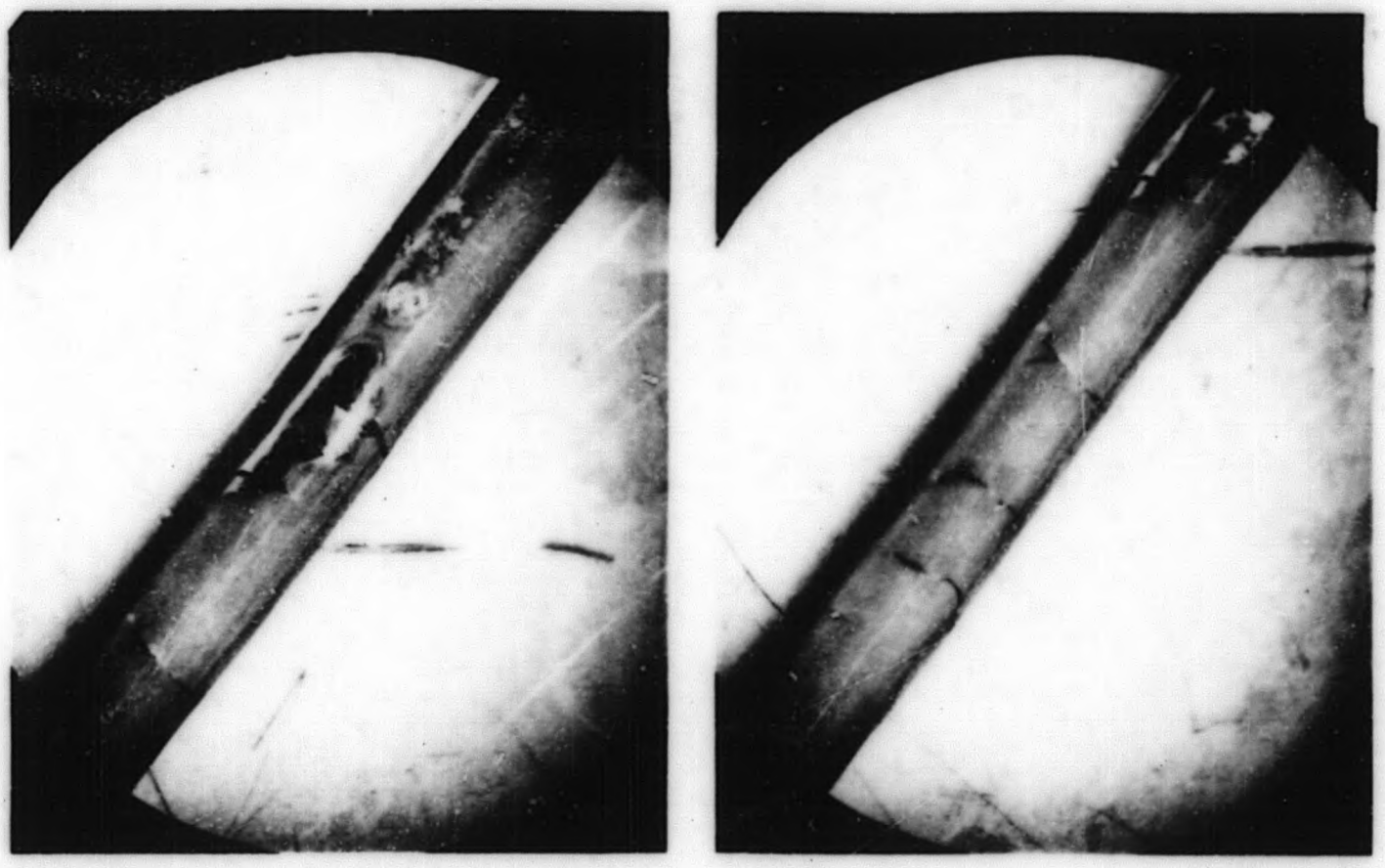

Circumferential cracks appear to be at or near pellet interfaces. This suggests that axial stress concentrations may have been present at these locations.

A metallographic section revealed that the cracks are intergranular. See Figures 52, 53, 54, 55 and 56.

Figure 51. Circumferential Cracks in Rod C, HPD 4E

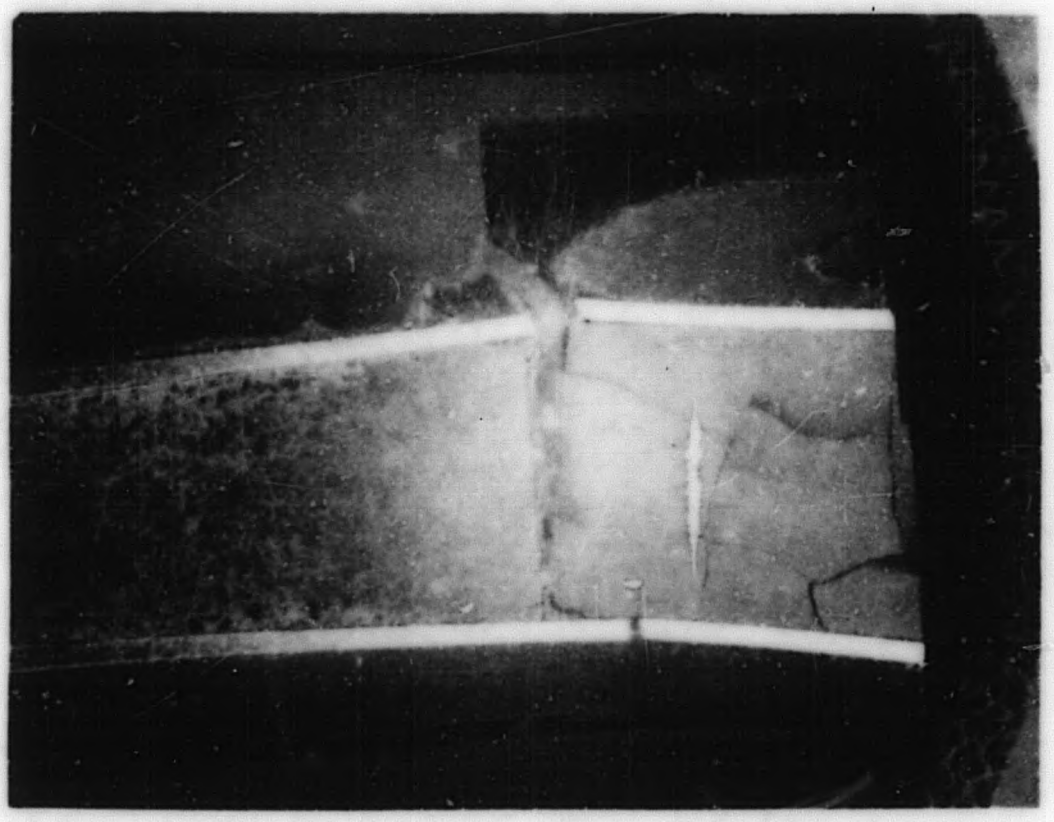

0.036 in. × 0.014 in. SS clad UO_2 pellets
0.005 nominal gap
Initial clad condition: Annealed 40,000 psi Y.S.
Failure location: Peak heat flux region
Exposure in failure location: 13,500 MWD/t
Heat flux in failure location: 460,000 Btu/hr-ft^2

Complete destructive exam in progress.

Figure 52. Circumferential Cracks in Rod C, HPD 4E

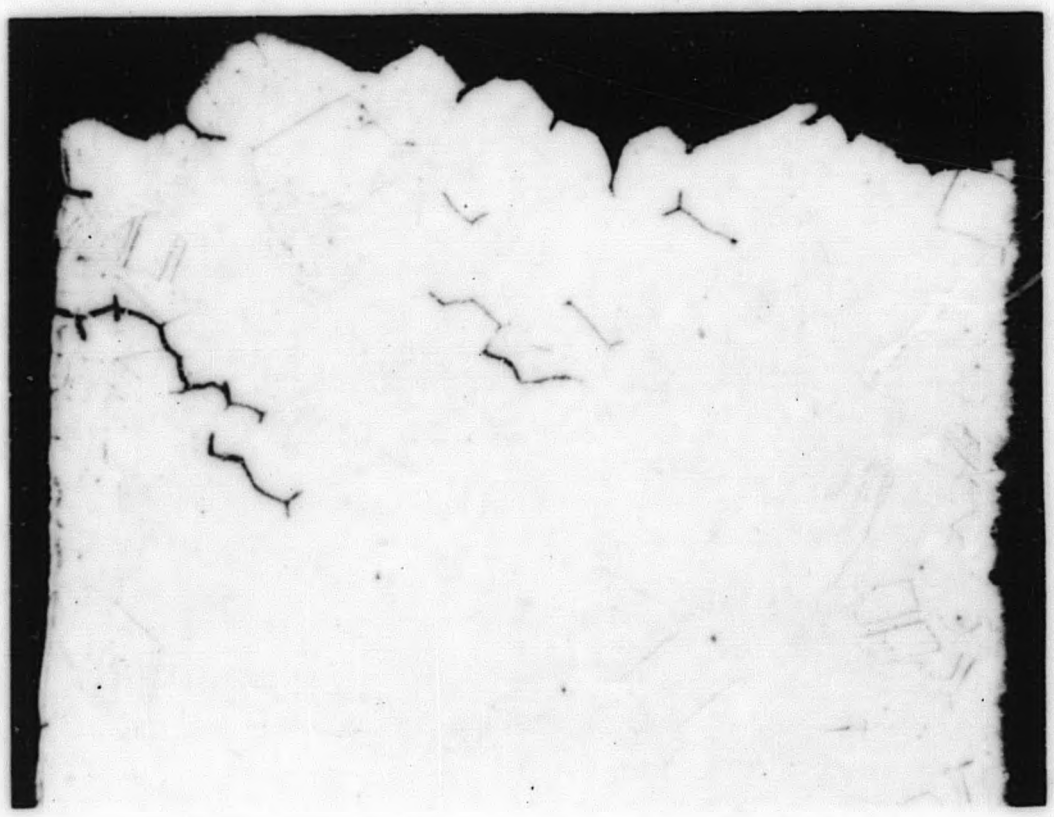

250× 8794-03

0.036 in. × 0.014 in. SS clad UO_2 pellets
0.005 nominal gap
Initial clad condition: Annealed 40,000 psi Y.S.
Failure location: Peak heat flux region
Exposure in failure location: 13,500 MWD/t
Heat flux in failure location: 460,000 Btu/hr-ft^2

Complete destructive exam in progress.

Figure 53. Circumferential Cracks in Rod C, HPD 4E

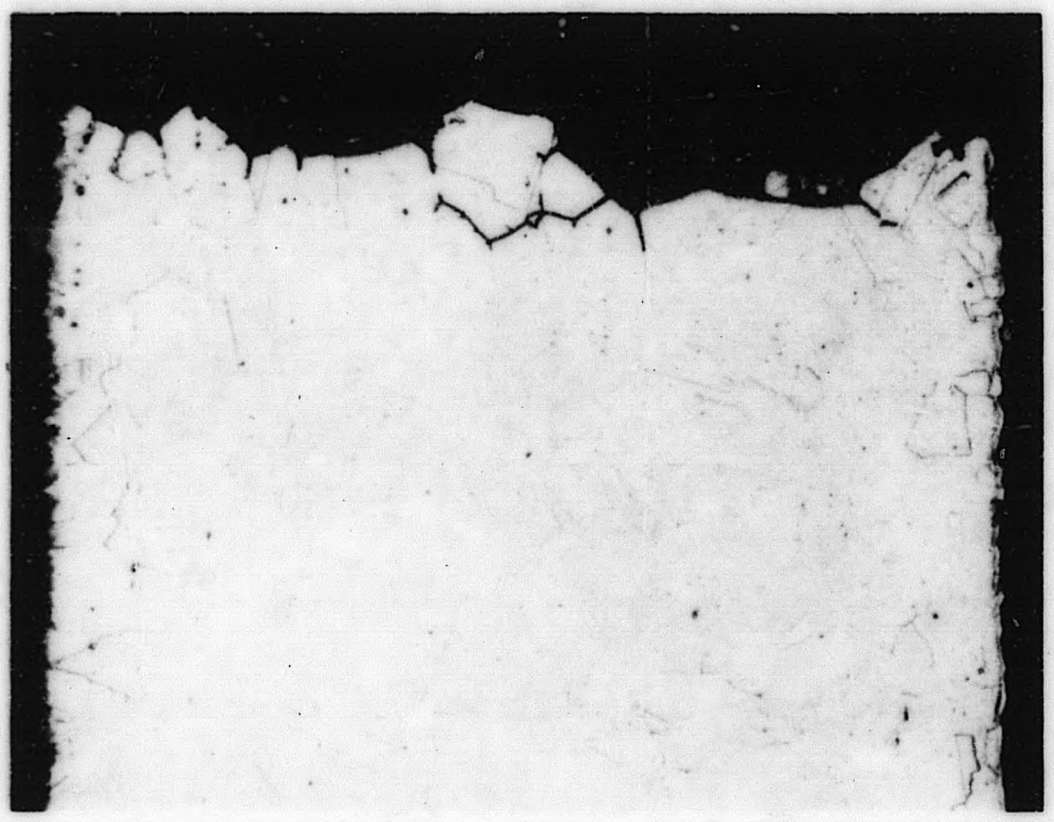

250× 8794-04

0.036 in. × 0.014 in. SS clad UO_2 pellets
0.005 nominal gap
Initial clad condition: Annealed 40,000 psi Y.S.
Failure location: Peak heat flux region
Exposure in failure location: 13,500 MWD/t
Heat flux in failure location: 460,000 Btu/hr-ft^2

Complete destructive exam in progress.

Figure 54. Circumferential Cracks in Rod C, HPD 4E

250× 8794-05

0.036 in. × 0.014 in. SS clad UO_2 pellets
0.005 nominal gap
Initial clad condition: Annealed 40,000 psi Y.S.
Failure location: Peak heat flux region
Exposure in failure location: 13,500 MWD/t
Heat flux in failure location: 460,000 Btu/hr-ft^2

Complete destructive exam in progress.

Figure 55. Circumferential Cracks in Rod C, HPD 4E

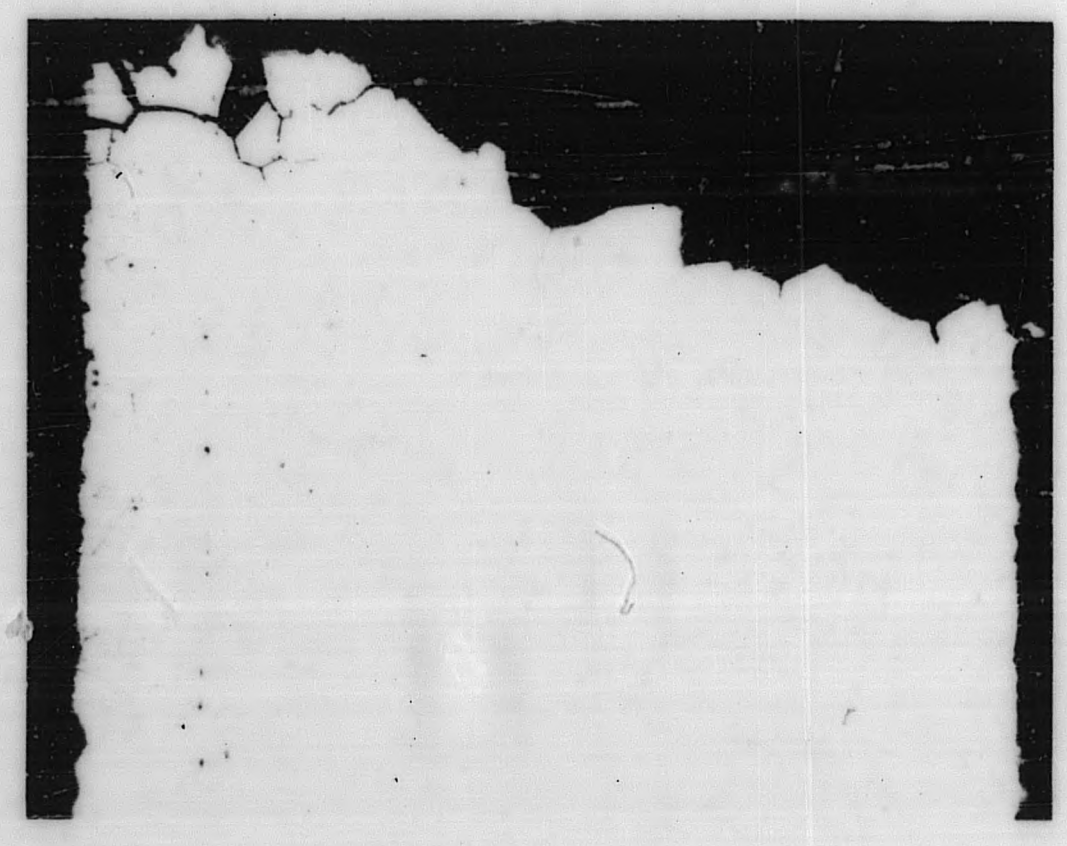

250× 8794-16

0.036 in. × 0.014 in. SS clad UO_2 pellets
0.005 nominal gap
Initial clad condition: Annealed 40,000 psi Y.S.
Failure location: Peak heat flux region
Exposure in failure location: 13,500 MWD/t
Heat flux in failure location: 460,000 Btu/hr-ft^2

Complete destructive exam in progress.

Figure 56. Circumferential Cracks in Rod C, HPD 4E

APPENDIX B

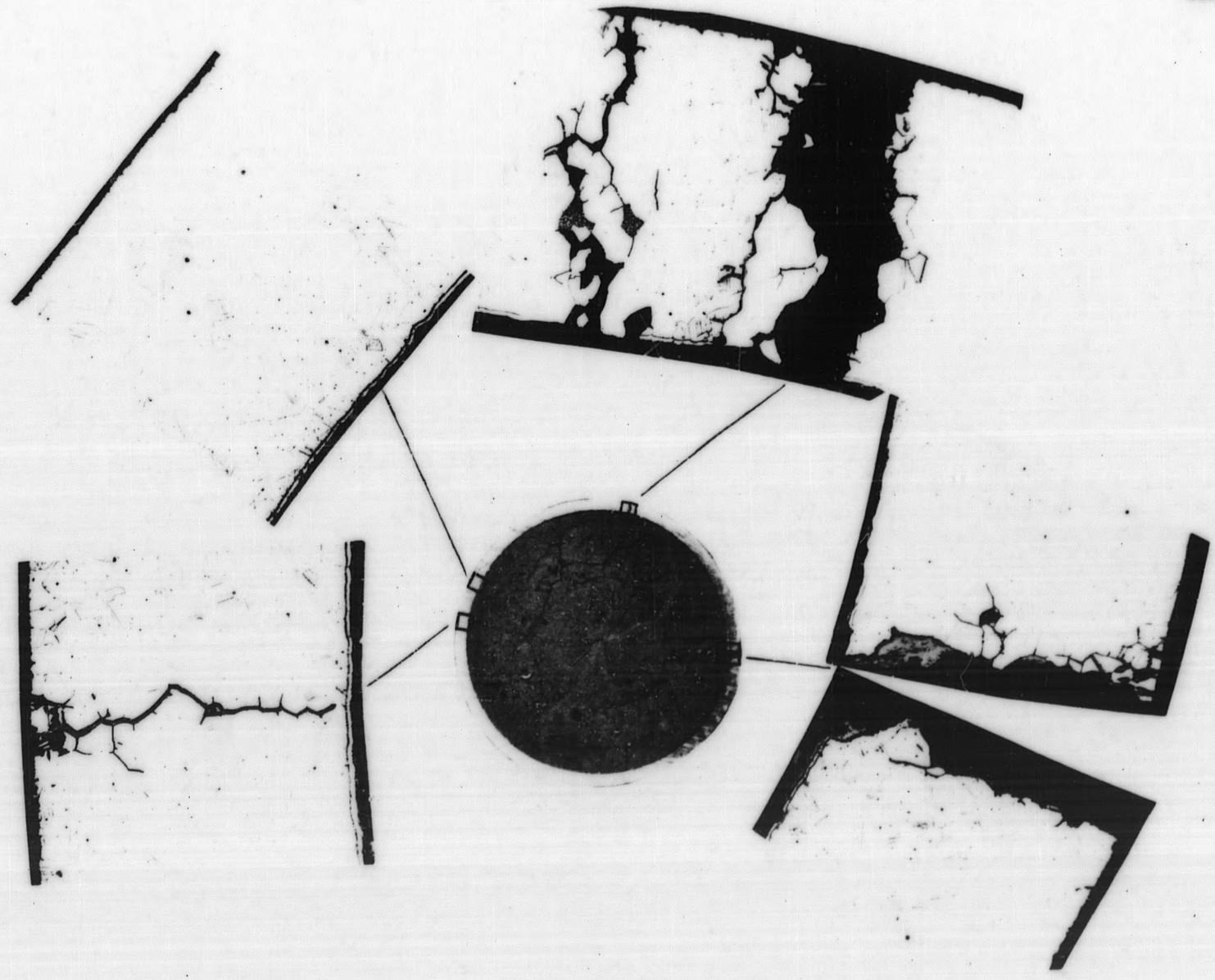

The appearance of intergranular cracking is shown. Notice the appearance of the large oxide "nugget" in photo on lower right. The appearance of this nugget is very similar to the one shown in Figure 35.

Figure 57. Cladding Defects in HPD 1E - Rod E

APPENDIX C

Appendix "C"

Pre-irradiation Chemical Analysis of Task 1A Fuel Cladding

Constituents Analyzed	Sample Number 1	2	3
H_2	10 ppm	40 ppm	5 ppm
N_2	10 ppm	10 ppm	28 ppm
O_2	150 ppm	780 ppm	155 ppm
W	100 ppm	100 ppm	100 ppm
Ti	500 ppm	500 ppm	500 ppm
V	100 ppm	500 ppm	500 ppm
Mg	100 ppm	100 ppm	100 ppm
Al	100 ppm	100 ppm	100 ppm
C	0.045%	0.11%	0.047%
Mo	0.16%	0.18%	0.17%
Cu	0.09%	0.11%	0.13%
Si	0.37%	0.37%	0.45%
Mn	0.60%	0.66%	0.72%
Cr	18.0%	18.0%	18.0%
Ni	9.1%	9.0%	9.0%

No trace of the following elements were found: Be, B, Ca, Zn, Ga, Ge, As, Y, Ag, Cd, In, Sn, Sb, Ba, La, Ta, Pb, Bi, Ce.

Samples: (1) Cold work 12 mil
(2) Annealed 14 mil
(3) Cold worked 14 mil

APPENDIX D

Appendix "D"

Pre-irradiation Chemical Compositions of 304 SS Cladding Used in Task 1B

Sample Identity	C	Mn	P	S	Si	Ni	Cr
8 mil Cold Worked	.05	1.54	.029	.019	.45	10.03	18.95
10 mil Cold Worked	.05	1.54	.029	.019	.45	10.03	18.95
15 mil Cold Worked	.022	1.57	.017	.015	.70	9.30	18.16
20 mil Cold Worked	.020	1.21	.022	.013	.55	9.39	18.95

The above data are taken from vendors' certified reports.

BIBLIOGRAPHY

1. Wanklyn, J. W., and Jones, D., "The Corrosion of Austenitic Stainless Steels under Heat Transfer in High Temperature Water", Journal of Nuclear Materials, 1, 154-173, July, 1959.
2. Snowden, P. P., "Stress Corrosion of Austenitic Stainless Steel by High Temperature Solutions and Contaminated Steam", Journal of Iron and Steei Institute, 194, 181-189, February, 1960.
3. Pashos, T. J., "Experience with Stainless Steel as a Fuel Cladding Material in Water Cooled Power Reactor Applications", APED-4260.
4. Fuel Cycle Program Twelfth Quarterly Progress Report, April-June, 1963, GEAP-4301.
5. N. S. Savannah Fuel Design and Development Program Quarterly Report, April 1, 1963, to June 30, 1963.
6. Brandt, F. A., Slosek, T. J. and Weidenbaum, B., "Irradiation and Examination of UO_2 High Burnup Program Fuel Elements", GEAP-3108, Part 3, January 15, 1962.
7. Nuclear Superheat Project Sixteenth Quarterly Report, May-July, 1963, GEAP-4332, August 15, 1963.
8. Fuel Cycle Program Thirteenth Quarterly Progress Report, July-September, 1963, to be published.
9. Naymark, S., Pashos, T. J., "Fuel Elements for Water Reactors, A Status Report", APED-4265, to be published.
10. Fowler, W. D., Lingafelter, J. W., "Design and Fabrication of High Power Density Fuel Assemblies for VBWR Irradiation Testing", GEAP-3609, November 1, 1960.
11. Lingafelter, J. W., "Fabrication of Fuel Rods by Tandem Rolling", GEAP-3775, July, 1961.
12. Lees, E. A., "Fabrication of Fuel Elements by Swaging", GEAP-3918, May 21, 1962.
13. DeHollander, W. R., "Vibrational Compaction of Uranium Dioxide", GEAP-4032, March 1, 1962.
14. Ryer, C. M., "Powder Fuel Processing by Two-Pass Swaging", GEAP-3891, April 10, 1962.
15. High Power Density Development Project Eighth Quarterly Progress Report, January through March, 1962, GEAP-3947, April 1, 1962.

16. High Power Density Development Project Ninth Quarterly Progress Report, April - June, 1962, GEAP-4044, July 1, 1962.

17. High Power Density Development Project Tenth Quarterly Progress Report, July - September, 1962, GEAP-4096, October 1, 1962.

18. High Power Density Development Project Eleventh Quarterly Progress Report, October - December, 1962, GEAP-4155, January 1, 1963.

19. High Power Density Development Project Twelfth Quarterly Progress Report, GEAP-4219, April 15, 1963.

20. High Power Density Development Project Thirteenth Quarterly Progress Report, GEAP-4309, June 15, 1963.

21. Lees, E. A., "Post Irradiation Examination and Evaluation of HPD 2S", to be published.

22. Osborne, R. N., "Locating Failed Fuel in Water Reactors", Nucleonics, July, 1961.

23. Rider, B. F., Russell, J. L., Jr., Harris, D. W., and Peterson, G. P., Jr., "The Determination of Uranium Burnup in MWD/T", GEAP-3373, March 17, 1960.

24. Womack, R. E., "Fission Gas Collection System", GEAP-3577, August, 1960.

25. Mathay, P. W., "Post Irradiation Examination of ORNL Maritime Fuel Assemblies 1A1 and 1A2", GEAP-3797, December, 1961.

26. Timoshenko, S., "Strength of Materials, Part II", Third Edition, D. Van Nostrano Company, 1956.

27. Crafts, Walter, and Lamont, John L., "Hardenability and Steel Selection", Pitman Publishing Co., 1949.

28. Spalaris, C. N., and Megerth, F. H., "Residual and Fission Gas Release from Uranium Dioxide". Published in American Nuclear Society Transactions, Volume 6, Number 1, June, 1963.

29. Fuel Cycle Program Monthly Progress Letter #27 for July, 1963, prepared for the Atomic Energy Commission, August 5, 1963.

30. HW 76228 Quarterly Progress Report, October, November, December, 1962, Metallurgy Research Operation, HAPO, January 15, 1963.

31. Lees, E. A., and Denison, W. L., "Residual Stresses and Stress Corrosion Cracking in Type 304 Stainless Steel", GEAP-4221.

ACKNOWLEDGEMENTS

The following have contributed materially in the conduct of the studies reported herein:

P. W. Mathay	RML
B. C. Beaudreau	RML
D. T. Ikeuye	RML
R. E. Smith	RML
P. J. Zamudio	VBWR
T. G. Lambert	Fuels and Materials
J. W. Lingafelter	Fuels and Materials

END